Hao *et al. Microstructures* **2025**, *5*, 2025012
DOI: 10.20517/microstructures.2024.10

Microstructures

Review

Open Access

Check for updates

Progress in *in situ* TEM investigations of halide perovskites

Lianzheng Hao, Songhua Cai

Department of Applied Physics, The Hong Kong Polytechnic University, Hong Kong 999077, China.

Correspondence to: Dr. Songhua Cai, Department of Applied Physics, The Hong Kong Polytechnic University, 11 Yuk Choi Road, Hung Hom, Kowloon, Hong Kong 999077, China. E-mail: songhua.cai@polyu.edu.hk

How to cite this article: Hao, L.; Cai, S. Progress in *in situ* TEM investigations of halide perovskites. *Microstructures* **2025**, *5*, 2025012. https://dx.doi.org/10.20517/microstructures.2024.10

Received: 31 Jan 2024 **First Decision:** 30 Apr 2024 **Revised:** 4 Jun 2024 **Accepted:** 22 Aug 2024 **Published:** 25 Jan 2025

Academic Editor: Xiaozhou Liao **Copy Editor:** Ping Zhang **Production Editor:** Ping Zhang

Abstract

Halide perovskites (HPs) have found wide-ranging applications in photovoltaic and optoelectronic devices, achieving remarkable success due to their unique crystal structure and properties. Given the sensitivity of perovskite materials to external stimuli, it is crucial to understand the intrinsic changes in structure and chemical composition during operational conditions. This understanding could assist researchers in exploring new strategies to enhance the photoelectrical properties and stability of these materials. While many *in situ* methods, such as *in situ* X-ray diffraction and *in situ* photoluminescence, have been employed to investigate the properties of perovskite materials in real-time, *in situ* transmission electron microscopy (TEM) stands out as an unparalleled technique for observing subtle changes at the micro and even atomic scale. In this review, we summarize recent advancements in studying HPs using *in situ* TEM. We first introduce studies on the crystallization process of HP crystals through *in situ* TEM observation, and then categorize research works on the degradation process of HPs driven by different external stimuli, including electron beam, heat, electrical bias, light, and ambient atmosphere. Finally, we highlight several challenges that still need to be addressed in the future. This review aims to present a thorough summary of the existing research and lay the groundwork for future inquiries in this captivating area.

Keywords: Halide perovskites, *in situ* transmission electron microscopy, crystallization, degradation

INTRODUCTION

Metal halide perovskites (HPs) have captured significant attention from the scientific community and

industrial investors due to their exceptional properties. These properties can be attributed to factors such as crystal structure, chemical composition, bonding motifs, and atomic configurations[1-3]. As a result, HPs found widespread application in photovoltaic and optoelectronic devices, including photodetectors, light-emitting diodes (LEDs), and solar cells[4-13]. Perovskite solar cells (PSCs), in particular, have been the focus of intense research in recent years. Since their first report in 2009, their certified efficiency has rapidly increased to 26.1% in just about ten years[14-16], which is comparable to single-crystal silicon solar cells. Additionally, perovskite LEDs and perovskite quantum dots (QDs)-based LEDs have also made remarkable strides. Cutting-edge green and red emission LEDs exhibit external quantum efficiencies (EQEs) exceeding 20%[17-20].

Generally, perovskite materials, used in photovoltaic or optoelectronic devices, belong to a category of materials with a chemical structure ABX_3, where A represents a monovalent cation, such as methylammonium ($MA^+ = CH_3NH_3^+$), formamidinium [$FA^+ = HC(NH_2)_2^+$], or Cs^+, B denotes the cation of lead or tin (Pb^{2+} or Sn^{2+}), and X signifies a halide anion (I^-, Br^-, or Cl^-).

The ideal structure of perovskite aligns with the cubic crystal system, specifically the face-centered cubic lattice, and comprises A and X ions in the closest packing of the cube. The smaller B ions fill 1/4 of the octahedral voids[21]. This structure allows for compositional designability and tunability through mixed-ion occupancy in the perovskite systems at each site. The geometrical Goldschmidt tolerance factor (τ) is used to determine whether the ions, with their varying radii, can form a stable perovskite structure. The acceptable range for this factor is 0.8-1[22-24]. Perovskite materials are characterized by a three-dimensional (3D) structure comprising corner-sharing octahedra and ionic bonds that can be polarized. This unique feature contributes to the soft ionic crystal properties of these materials, making them susceptible to changes in both surface and bulk structures when in polycrystalline forms. Moreover, the composition and structure of perovskite materials can be readily modified, leading to intriguing and customizable optoelectronic properties. However, these adaptable characteristics also present challenges in fully understanding their properties at an atomic level. Deepening our comprehension of the atomic structures of these materials and establishing the corresponding relationships between structure, property, and performance will propel the advancement of high-performance, durable optoelectronic technologies based on next-generation perovskites.

In the field of materials science, a crucial element involves comprehending the properties of materials and their impact on device performance by examining their underlying structures and transformations. A range of characterization techniques are available to delve into the fundamental attributes of perovskite semiconductors, including their morphological features, crystal structures, band gaps, elemental composition, and charge carrier dynamics[25-31]. Hybrid composition perovskite semiconductors, also known as HPs, are ionic compounds with low formation energy. This makes them prone to defect formation during nucleation and crystal growth processes[32,33]. These defects can adversely affect the optical and electrical characteristics and the operational stability of HPs. Consequently, there is a pressing need for detailed and precise observations at the atomic level, considering the relationship between structure, properties, and performance. By gaining a thorough understanding of the inherent composition, microscopic interfaces, internal grain imperfections, and interfacial characteristics of perovskites, the development of high-performance optoelectronic devices using HPs can be significantly accelerated. Therefore, it is vital to establish a fundamental correlation between structure and properties, particularly when investigating the micro and atomic aspects.

Transmission electron microscopy (TEM) has proven to be a powerful and indispensable tool for material characterization, thanks to its ultra-high spatial resolution (less than 1 Å), temporal resolution (less than 1 ms), and energy resolution (less than 0.1 eV)[34-38]. This is achieved by utilizing high accelerating voltage (ranging from 60-300 kV) for the electron beam, which results in extremely short wavelengths and enhances the spatial resolution of TEM. The integration of new technologies, such as the direct-detection electron-counting (DDEC) camera and high-frame-rate (HFR)[39,40], facilitates the capture of high-resolution TEM (HRTEM) images with both low electron beam dose requirements and high-temporal resolution. Additionally, scanning TEM (STEM) is a variant of TEM where the electron beam is focused to a fine spot (typically 0.05-0.2 nm in size) and then scanned over the sample in a raster illumination system. This feature makes STEM suitable for analytical techniques such as Z-contrast annular dark-field imaging, and mapping through spectroscopic methods such as energy dispersive X-ray (EDX) spectroscopy or electron energy loss spectroscopy (EELS). Most importantly, the integration of an aberration corrector into STEM allows electron probes to be focused to sub-angstrom diameters, thereby enabling the acquisition of sub-angstrom resolution images. Additionally, Direct Electron Detectors (DEDs) have been employed[41], demonstrating a tenfold improvement in detection quantum efficiency. This has led to an unprecedented increase in the signal-to-noise ratio (SNR), along with a significantly faster acquisition speed compared to traditional Charge-Coupled Device (CCD) cameras[42]. The development of the integrated differential phase contrast (iDPC) method, based on segmented STEM detectors, represents a significant advancement in the realm of low-dose STEM imaging[43]. Furthermore, four-dimensional STEM (4D-STEM), a novel and efficient approach for low-dose imaging, stands out. It collects a wealth of information from both real and reciprocal spaces, and by leveraging the redundancy in the data, 4D-STEM facilitates the retrieval of high-quality images[44]. This effectively broadens the scope of applications for materials that are sensitive to electron beams. Establishing a fundamental correlation between atomic scale structure, properties, and performance using TEM has posed a significant challenge, primarily due to the sensitive nature of HPs[45-49]. However, recent advancements in low-dose imaging technology have simplified the process of obtaining high-resolution images of these beam-sensitive materials. Over recent years, there has been considerable progress in applying TEM characterization to analyze HPs.

Preparing an appropriate specimen is a prerequisite for conducting reliable TEM experiments. Generally, there are three primary methods for preparing HP samples for TEM analysis. (1) Focused ion beam (FIB) processing technique: The FIB technique is widely used in fabricating HP specimens, offering the flexibility to examine any specific area within HPs using TEM. By employing ion beam milling, the sample thickness can be conveniently reduced to meet the necessary criteria for TEM analysis. However, it is important to note that using high-energy ion beams can cause permanent structural damage to the sample, presenting a significant drawback for HPs. To mitigate this issue, strategies such as decreasing the ion beam intensity, accelerating voltage, and reducing the processing temperature have proven successful; (2) Blow-assisted spin coating method: This process involves preparing samples directly on TEM copper grids by applying a diluted precursor solution and using spin-coating. In the standard spin-coating method, researchers typically use antisolvent to promote the rapid crystallization process. However, applying the antisolvent is not an easy method to obtain a sample with high crystal quality. Instead, some researchers have reported that using uniform airflow can substitute the effect of antisolvent and yield a high-quality sample[50]; (3) Ultrasonication solution technique: The ultrasonication solution technique is widely used to quickly prepare zero- (0D), one- (1D), and two-dimensional (2D) HP samples for TEM analysis. Known for its simplicity and efficiency, this technique eliminates the need for complex additional processing procedures. Currently, it is the most common method for preparing HP samples for TEM examination. Moreover, various strategies have been proven effective in mitigating the damage caused by beam irradiation to HPs. For instance, applying a protective layer on the surface has been shown to decrease the impact of electron beam penetration on HPs[51]. Another approach involves incorporating Mn elements into the host structure of

HPs through doping techniques, which enhances the stability of HPs by strengthening the Mn-Cl and Pb-Cl bonds[47]. In terms of modifying TEM imaging conditions, although using a low-energy electron beam at a reduced accelerating voltage is considered as an efficient method to minimize structural damage resulting from energy transfer, this method may not be so effective when it comes to HPs. Chen *et al.* proposed that low acceleration voltage is ineffective or even harmful in protecting the perovskite crystal structure[52]. Lowering the electron dose has been confirmed as the most applicable approach for mitigating electron beam damage to HPs. Besides, some research works also utilize cryogenic conditions to further enhance HPs' tolerance to electron irradiation[53,54]. However, low-dose observation may somewhat compromise the SNR and spatial resolution of the TEM image. Fortunately, the use of the DDEC camera and direct electron detection detectors brings new hope to this field, as it can obtain high-quality images at low beam doses.

Initially, the application of TEM characterization was confined to observing large morphological changes, which appeared blurry under low magnification, or confirming the formation of Pb nanoparticles (NPs) following the decomposition of HPs induced by the electron beam[55,56]. In 2017, Rothmann *et al.* made a groundbreaking discovery of prevalent twin crystal structures in perovskite films by analyzing selected area electron diffraction (SAED) patterns[50]. Later, Chen *et al.* provided a comprehensive elucidation of the step-by-step decomposition process of $MAPbI_3$ through diffraction analysis[57]. Notably, Doherty *et al.* began exploring the often-overlooked non-cubic phase structural characteristics from the FA-rich structure by utilizing the electron diffraction (ED) pattern extracted from a scanning ED (SED) measurement[58]. Regarding the direct observation of the atomic arrangement of delicate organic-inorganic HPs, such as STEM and HRTEM imaging models, significant initial progress was made by Zhang *et al.* They employed various low-dose TEM imaging techniques to observe $FAPbI_3$ perovskite at the atomic scale[40]. Building on this, Rothmann *et al.* were able to capture the atomic arrangement of organic-inorganic HPs using a low-dose STEM imaging mode. At the atomic level, they could vividly visualize corresponding points, interfaces, line defects, and grain boundaries[59]. Furthermore, to enhance the structural robustness of HPs when exposed to electron beams, the incorporation of cryo-electron microscopy (cryo-EM) into the process of structurally characterizing HPs has been introduced[53]. In addition to 3D HPs, STEM and HRTEM have also been used to characterize low-dimensional HPs, such as 2D HPs and perovskite QDs[60-67]. For example, Jung *et al.* first observed the atomic structure of 2D Ruddlesden-Popper $BA_2MA_2Pb_3I_{10}$ perovskite[61]. Ning *et al.* confirmed the existence of QDs in perovskite solids using HRTEM images and corresponding SAED patterns[60]. Otero-Martínez *et al.* observed the atomic structure of $(K_{0.18}Cs_{0.82})_4PbBr_6$ nanocrystal using high-angle annular dark field (HAADF)-STEM[67].

While static TEM observation has provided comprehensive insights into the underlying microstructures of HPs, it falls short in capturing the dynamic changes of the materials under external stimuli. To bridge this gap, *in situ* TEM characterization is employed, enabling real-time monitoring of ion migration, microstructural changes, phase transitions, and alterations in the microstructure of HPs under varying external conditions[68-71]. This technique paves the way for exploring the yet-undiscovered behaviors of HPs. *In situ* TEM characterization can replicate the actual operating conditions of specimens by employing various external stimuli, including but not limited to temperature, moisture, cryogenics, oxygen, light, electric fields, and magnetic fields. By meeting this condition, it becomes possible to conduct a thorough examination of specimens within a specific ecological setting. Currently, *in situ* observation in TEM is primarily achieved through two approaches. One is environmental TEM (ETEM), which features a special specimen chamber that can provide various atmospheric environments[72,73]. The other is through a specially designed *in situ* specimen holder that can also provide external stimuli using technologies such as micro-electro-mechanical systems (MEMS)[74,75]. In recent times, there has been notable advancement in the *in situ* TEM technique, leading to its widespread utilization in various fields of functional materials

research. These fields include the development of high-strength alloys, electrode materials with high specific energy, and high-performance catalysts, among others[71,76,77]. Organic-inorganic HPs possess delicate crystal structures, which pose difficulties in performing *in situ* TEM experiments. Nevertheless, a number of groundbreaking *in situ* TEM investigations have already been conducted on HPs, unveiling significant advancements in the utilization of this technique. In light of this, we present a comprehensive overview of the scientific breakthroughs facilitated by *in situ* TEM, with a specific emphasis on its effectiveness in addressing the key obstacles encountered in studying HPs. Lastly, we also propose challenges that still require considerable effort in this area.

CRYSTALLIZATIONS OF HPS

The performance of HP devices largely depends on the quality of the absorption layer, which in turn relies on the crystallization of the HP film. However, cultivating high-quality absorption HP films from solutions is complex, as synthetic conditions can significantly influence the film's quality. Absorption layers characterized by compositional segregation, high defect concentration, and poor morphology can substantially decrease device performance[27,78-80]. Therefore, it is crucial to investigate the underlying crystallization process to enhance the production of premium HP films, which play a vital role in large-scale device manufacturing across various industries. Most perovskite materials are fabricated using the solution method, and a special holder is needed to study the crystallization process. The use of liquid-cell TEM allows for the direct and real-time observation of dynamic processes occurring in liquid environments. By employing this technique, the limitations associated with traditional *ex situ* TEM analysis are bypassed, thus facilitating a better understanding of the formation and dynamics of NPs in their original solutions[81]. Additionally, HRTEM generally requires a high vacuum environment to prevent gas molecules within the column from scattering the accelerated electrons, which could significantly degrade the image resolution. However, materials can exhibit different behaviors under various atmospheric conditions compared to a high vacuum. This discrepancy has necessitated the introduction of specific atmospheres into the TEM specimen chamber during operation. To date, two primary methods have been proposed: the aperture method, which relies on a specially constructed gaseous sample chamber in the TEM (also known as the ETEM method), and the window method, which employs a custom TEM holder with a MEMS-based nanoreactor (also referred to as the gas holder method)[82-84].

Due to its unique crystal structure, the crystallization process of HPs includes not only nucleation and growth but also phase transition[85]. At room temperature (RT), the formed perovskite material usually has an orthorhombic phase that lacks photoelectrical properties. Therefore, after the nucleation and growth process, the perovskite grains generally need to undergo a phase transition process from the orthorhombic phase to the tetragonal or cubic phase. Moreover, the precursor solution is typically dissolved by polar solvents, such as dimethylformamide (DMF) and dimethyl sulfoxide (DMSO). These solvent molecules can coordinate with Pb^{2+} and form an intermediate phase. Consequently, studying the transition process can provide a deeper understanding of the material. In this chapter, we explore the application of *in situ* TEM for studying the crystallization process of HPs through two main aspects: nucleation and growth, and phase transition.

Nucleation and growth

Nucleation is the first step in the crystallization process, and it largely determines the film quality. In 2016, Qin *et al.* first investigated the crystallization process of $CH_3NH_3PbI_3$ ($MAPbI_3$) using *in situ* liquid-cell TEM[86] [Figure 1A]. Initially, they demonstrated the effectiveness of using electron beam-induced solvent evaporation to directly precipitate $MAPbI_3$ from precursor solutions. The compact structural configurations of the $MAPbI_3$ NPs enable them to have a high tolerance to electron irradiation. However, it remains

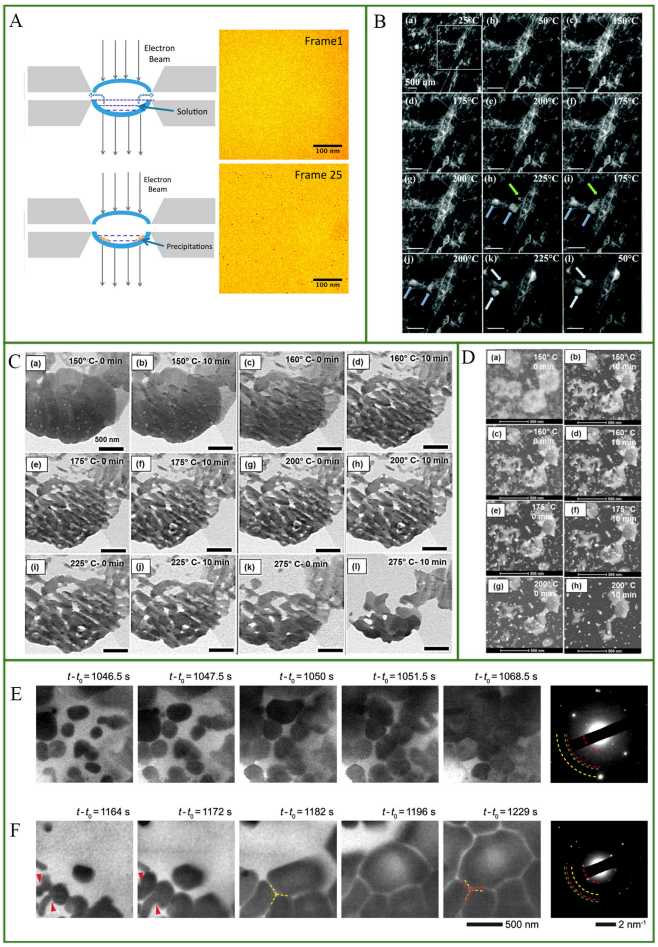

Figure 1. (A) The schematic diagram on the left side of the image shows the formation of hybrid organic-inorganic perovskite precipitation through the electron beam-assisted solvent evaporation method. The right side of the image displays two consecutive frames captured during TEM imaging of the $MAPI_3$ samples at a dose rate of 86 $e^-/(Å^2\ s)$ per frame. Reproduced with the permission of Ref.[86] Copyright © 2016 American Chemical Society; (B) *In situ* TEM characterization exhibiting the evolution of $FAPbI_3$ film structure over time and temperature. Reproduced with the permission of Ref.[55] Copyright © 2016 Royal Society of Chemical; (C) The bright field (BF) images show the nucleation process at different temperatures with water partial pressure of about 1 mbar measured at room temperature (RT); (D) The dark field images show the effect of high humidity on the nucleation process at different temperatures. The water partial pressure is about 10 mbar measured at RT. Reproduced with the permission of Ref.[90] Copyright © 2016 American Chemical Society; (E) Sequential *in situ* TEM images captured from various sections of a heated liquid cell at 90 °C depict the progression of perovskite nanocrystals transforming into consistent thin films under conditions of both high and low (F) nucleation densities, respectively. For these SAED images, dashed red, green, orange, and yellow quarter circles correspond to {110}/{220}, {213}, {202}, and {400} planes of the tetragonal perovskite crystal. Reproduced with the permission of Ref.[91] Copyright © 2022 American Chemical Society. TEM: Transmission electron microscopy; SAED: Selected area electron diffraction.

necessary to maintain a dose rate of less than 90 $e^-/(Å^2\ s)$ to prevent or minimize beam damage. By quantitatively analyzing the evolution of NPs in the solution, they discovered that the average NP radius (R_a) and time (t) follow a relationship approximately characterized by $Ra \sim t^{1/5}$. This relationship does not completely align with either the diffusion or reaction-limited growth models predicted by the Lifshitz-Slyozov-Wagner (LSW) theory[87-89]. They observed the frequent coalescence phenomenon in solution regions with a high density of precipitates, demonstrating complex dynamical behaviors. To better understand this intriguing occurrence, they proposed an integrated approach considering both crystal orientations and chemical characteristics. This study presents a technique using liquid-cell TEM methods to investigate the nucleation and growth characteristics of organic-inorganic hybrid materials. The approach

developed in this research lays the foundation for future comparative studies on hybrid organic-inorganic perovskites composed of different anions (e.g., Cl and Br) and cations (e.g., FA and Cs).

Nearly simultaneously, Aguiar *et al.* performed a series of *in situ* TEM experiments to investigate the crystallization behavior of $FAPbI_3$ perovskite under elevated temperatures[55]. Their research yielded significant insights into the mechanisms governing perovskite formation and degradation, particularly regarding grain morphology evolution and interfacial chemical reactions. Figure 1B illustrates that the optimal processing temperature for $FAPbI_3$ occurs at 175 °C. Notably, the grain boundaries exhibit a higher lead content compared to the grain interiors. At this temperature, a partially reversible process occurs, involving the lead exchange between the inner and surface boundaries. Beyond 175 °C, the formation and growth of lead-rich precipitates become evident. Nevertheless, these precipitates can only be partially reintegrated into the material after extended annealing at the same temperature. Additionally, through a thorough microstructural analysis, it was confirmed that the absorption of both hydrogen and hydroxide ions occurs readily at the grain interfaces. This absorption phenomenon can be ascribed to the presence of residual water vapor trapped within the non-crystalline substance at the grain boundaries during the formation process. This discovery provides insight into the intrinsic mechanisms underlying the formation and degradation of HPs under humid conditions.

In 2016, Aguiar *et al.* conducted a series of controlled *in situ* gas experiments using a differentially pumped ETEM equipped with a heating stage[90]. This experimental setup allowed for direct observation of the crystallization process of FA-based perovskite in the presence of water vapor, nitrogen, and oxygen gases. Under these conditions, the combination of low temperature and water vapor pressure did not significantly alter the precursor materials [Figure 1C]. Building upon these observations, they proposed a mechanism for the crystallization and solidification phenomenon in organic-inorganic perovskites, which involves a thermal process within a nonreactive atmosphere. Their hypothesis suggests that the system minimizes its free energy by reducing the free surface area as crystals grow. Furthermore, they proposed that recrystallization occurs along grain boundaries, where any residual water inhibits crystallization and grain growth in the absence of sequential annealing. Additionally, to explore the impact of high humidity on the crystallization process of $FAPbI_3$ under ambient conditions, they conducted *in situ* ETEM experiments using a water pressure of 10 mbar at RT. Figure 1D displays the evolution process in a dark field image. They observed rapid material degradation and loss under 1 mbar of water pressure after annealing at 200 °C for ten minutes. However, under 10 mbar of water pressure, no significant degradation occurred at the same temperature. They also observed crystal coarsening under these two different water pressures. Furthermore, they discovered that the crystallization process is similar under both argon and air atmospheres. Consequently, they concluded that the formation of perovskite materials through crystallization remains unaffected by the surrounding gas environment. This study showcased the crystallization process under water vapor and environmental gases, providing a crucial foundation for future research.

In a later study, Wang *et al.* employed *in situ* liquid-phase TEM to trace the nucleation process of $MAPbI_3$ from a precursor solution[91]. The perovskite precursor solution was spin-coated onto a silicon nitride (SiN_x) window within an *in situ* liquid chip and heated to 90 °C. As depicted in Figure 1E, perovskite films formed through the aggregation of nanocrystals originating from the substrate surface. The growth of perovskite nanocrystals continued until they contacted each other, covering the entire available substrate surface (t - t_0 = 1164 - 1196 s). Subsequently, grain growth decelerated and eventually ceased. In another region of the liquid cell [Figure 1F], smaller nanocrystals merged to create larger single-crystal grains. Notably, images captured during the later growth phase (t - t_0 = 1229 s) revealed transformations in grain boundaries, leading to adjustments in the angles between grains at triple junctions. This phenomenon was attributed to

the principle of minimizing grain boundary energy, resulting in equalized dihedral angles and enhanced grain boundary configurations. Additionally, the researchers explored mechanisms by which additives such as urea influence perovskite formation, leading to increased grain size. They observed that perovskite nanocrystals exhibited higher solubility in a precursor solution containing urea. This solubility enhancement was ascribed to coordinate bonds forming between Pb^{2+} ions in the perovskite and oxygen (O) in urea, weakening the Pb-I bond and elevating perovskite solubility. Their method of investigating perovskite film development provides valuable insights for enhancing the production of perovskites and other technologically significant crystalline films.

These *in situ* TEM studies reveal the detailed crystallization process and its influencing factors in HPs. While these results provide a microscopic view of the entire process within a range from micrometers to several hundred nanometers, there is still a lack of in-depth nanoscale characterization to reveal more structural details. It is expected that exploring the crystallization behaviors at the nanoscale or even the atomic scale-considering factors such as domain structures, grain boundary arrangements, uniformity of the perovskite phase, and defect-induced strain-may bring insights into the underlying mechanisms.

Phase transition

As previously mentioned, perovskite crystals formed at RT typically undergo a phase transition process. This transition significantly influences the final crystal quality and photovoltaic property. Therefore, gaining a detailed understanding of this transition process can enhance our comprehension of the properties of HPs. In an inorganic HP system, Zhang et al. investigated the phase transition process under different temperatures in a $CsPbBr_3$ single crystal[92]. Initially, they identified two types of growth twin domains within the $CsPbBr_3$ crystal. Subsequently, they explored the relationship between growth twin domains and transformation twins using *in situ* TEM. By analyzing SAED patterns [Figure 2A], they confirmed the phase transition temperature for a single $CsPbBr_3$ crystal. The $CsPbBr_3$ crystal exhibited an orthorhombic structure at RT. As the temperature increased to 90 °C, it transformed into a tetragonal structure and further transitioned to a cubic structure at 133 °C. Notably, an intriguing phenomenon emerged-the evolution of twin domain walls. Figure 2B illustrates that the $CsPbBr_3$ crystal displayed a distinct twin domain feature at RT. However, as the temperature rose from RT to 120 °C, the boundaries between crystal domains gradually blurred due to slight orientation deviations caused by thermal drift. Surpassing 133 °C, the domain boundaries abruptly vanished, precisely coinciding with the temperature of the first-order phase transition. Upon cooling, the lamellae reappeared but were now horizontally oriented. This peculiar memory effect observed in the crystal twins suggests that the domains formed during crystal growth and phase transition exhibit ferroelastic properties. These domains effectively divide the crystal into distinct orientation states, which can be either identical or enantiomorphous in structure, differing in their inherent spontaneous strain characteristics. The researchers proposed that the transition of the sample to a cubic structure signifies complete relaxation of the spontaneous strain induced by structural distortions, resulting in the simultaneous disappearance of domain boundaries. Conversely, during cooling, as strain intensifies with decreasing temperature, domain walls emerge to minimize the total system energy. The SAED pattern before and after heating reveals a transformation of the twin relation from reflection twins to 90° rotation twins along $[10\bar{1}]$. They interpreted this formation of domain walls due to energy minimization during the phase transition. Consequently, $[10\bar{1}]$ rotation twins, possessing lower domain wall energy, are favored. Their research not only deepens our understanding of the imperfections in $CsPbBr_3$ but also paves the way for more refined applications in photovoltaics, offering a pathway for customization.

One of the advantages of HPs in the field of photoelectron lies in their ease of fabrication using solution methods. DMF and DMSO are two widely used polar solvents for dissolving raw materials. However, research has revealed that employing these two coordinating solvents leads to the formation of solvated

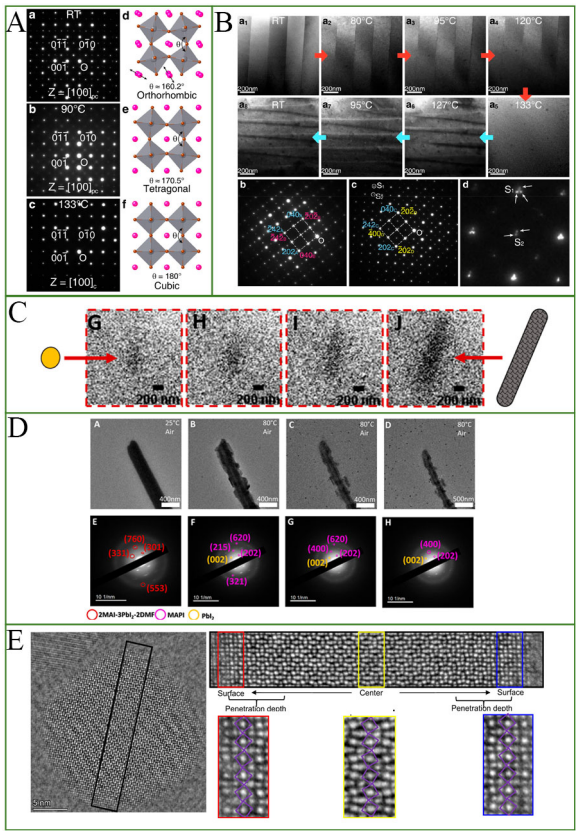

Figure 2. (A) The SAED patterns of $CsPbBr_3$ were captured at three different temperatures: at RT, at 90 °C, and at 133 °C, respectively; (B) TEM images show the morphology of the domain varies *in situ* as the temperature rises from RT to 133 °C, followed by cooling, and the corresponding SAED patterns. Reproduced with the permission of Ref.[92] Copyright © 2020 American Chemical Society; (C) TEM images show the nucleation and growth processes of the 2MAI-3PbI_2-2DMF intermediate; (D) TEM images and corresponding SAED patterns show the phase transition process. Reproduced with the permission of Ref.[96] Copyright © 2023 American Chemical Society; (E) DPC-STEM image of a single $CsPbI_3$ nanocrystal heated at 200 °C viewed from the [001] direction and the magnified images from the colored box, showing the phase transition dynamics. Reproduced with the permission of Ref.[97] Copyright © 2023 Springer Nature. SAED: Selected area electron diffraction; RT: Room temperature; TEM: Transmission electron microscopy; DPC-STEM: Differential phase contrast-scaning transmission electron microscopy.

intermediates[93-95]. Consequently, Sidhoum *et al.* aimed to elucidate the evolution process-from precursor solution to solvated intermediates, and ultimately to perovskite-using *in situ* liquid and gas TEM[96]. Initially, they filled the *in situ* liquid cell with toluene and then injected the perovskite precursor, resulting in precipitation. As depicted in Figure 2C, nuclei gradually appeared and grew into rod-like structures. Additionally, they conducted Small- (SAXS) and Wide-Angle X-ray scattering (WAXS) experiments, confirming that the intermediate species is 2MAI-3PbI_2-2DMF. Furthermore, they leveraged the *in situ* TEM chip to directly observe the phase transition of the intermediate. To simulate real experimental conditions during the transition process, they injected ambient air from the room into the TEM sample holder, maintaining a temperature of 80 °C. The phase transition process is illustrated in Figure 2D. After annealing for 45 min at 80 °C, the intermediates transformed completely into tetragonal perovskite. This work provides conclusive and unique evidence of crystal fragmentation concurrent with the structural transition from the intermediate to the final phases.

Previous studies investigating phase transitions primarily relied on morphological changes and SAED patterns, falling short of achieving atomic resolution characterization. However, thanks to emerging

low-dose technology, genuine atomic resolution imaging can now be accomplished through *in situ* TEM characterization, providing a deeper understanding of the relationship between structure and performance. Ma *et al.* applied iDPC-STEM to observe the phase transition of $CsPbI_3$ nanocrystals with atomic resolution in real-time for the first time[97]. They tracked the phase transition of α, β, and γ phases of $CsPbI_3$ nanocrystals at atomic scale across temperatures ranging from RT to 250 °C. More significantly, they discerned the gradual phase transition process from the surface to the center within a single $CsPbI_3$ nanocrystal. As depicted in Figure 2E the rotation angles of PbI_6 octahedrons, indicative of the extent of phase transition, were larger at the center than near the surfaces. This continuous distribution of the perovskite phase likely spans from γ (center) to near α (surface). Notably, this outcome suggests that the heat impact infiltrated the nanocrystal progressively rather than occurring abruptly throughout its entirety. These findings provide detailed insights into the atomic-level changes during the transition dynamics of perovskite phases, revealing a gradual transition process over a significant period, characterized by distinct intermediate stages and spatial arrangements.

In *in situ* TEM observations of HP phase transition processes, technical advantages bring new opportunities for in-depth understanding. Initially, researchers relied on morphological changes and SAED patterns to study these transitions. However, as low-dose technology advances, researchers can now directly capture the gradual evolution process of phase transitions with high spatial resolution using iDPC-STEM. Despite these advancements, most studies still focus primarily on the phase structure isolatedly. It is well-known that domain structures tend to disappear when a perovskite phase with high symmetry transforms into a lower-symmetry phase. This transformation can lead to the generation and interaction of lattice strain, yet its impact on perovskite material performance remains unclear. Additionally, defects may arise during the phase transition process. Therefore, it is preferred to employ a combination of imaging and analytic techniques, such as cathodoluminescence spectroscopy (CL), DPC, 4D-STEM, and EELS, to obtain more physical information on domain boundaries and defects related to perovskite performance.

DEGRADATIONS OF HPS

Due to the weak ionic properties of HPs, they exhibit relative sensitivity to external stimuli, which can adversely affect device stability. Understanding the impact of these external stimuli on HPs is crucial. Numerous researchers have conducted extensive studies to investigate the decomposition mechanisms of HPs. In this section, we primarily categorize these mechanisms based on the type of external stimuli.

Electron beam

Due to the weak ionic properties of HPs, they are susceptible to unavoidable secondary and radiolysis damage, which accelerates their degradation in TEM, thereby complicating the analysis of observed phenomena. When exposed to electron beam irradiation, halogen ions rapidly detach from the structure, and organic components readily decompose due to radiolysis, leading to structural collapse. Consequently, the primary task before conducting TEM experiments is to determine a safe dose to avoid observing distorted images. Wu *et al.* have summarized safe and damaging doses for different perovskite materials under TEM observation[98]. Extensive investigation has been conducted regarding the deteriorating effects of electron beam exposure on HPs, with the prevailing notion attributing degradation to phase segregation and transition phenomena. Dang *et al.* conducted a research investigation to observe the effects of electron beam irradiation on the radiolysis process of $CsPbBr_3$[56]. As depicted in Figure 3A, they found that with increasing electron beam dose, significant changes in $CsPbBr_3$ nanocrystal morphology were evident from HAADF-STEM images. Furthermore, EDX measurements indicated that the intensities of Cs and Pb remained relatively unchanged, while a decrease in Br intensity was observed, particularly at higher electron doses. The reduction in the number of Br atoms can be attributed to the desorption of ionic compounds

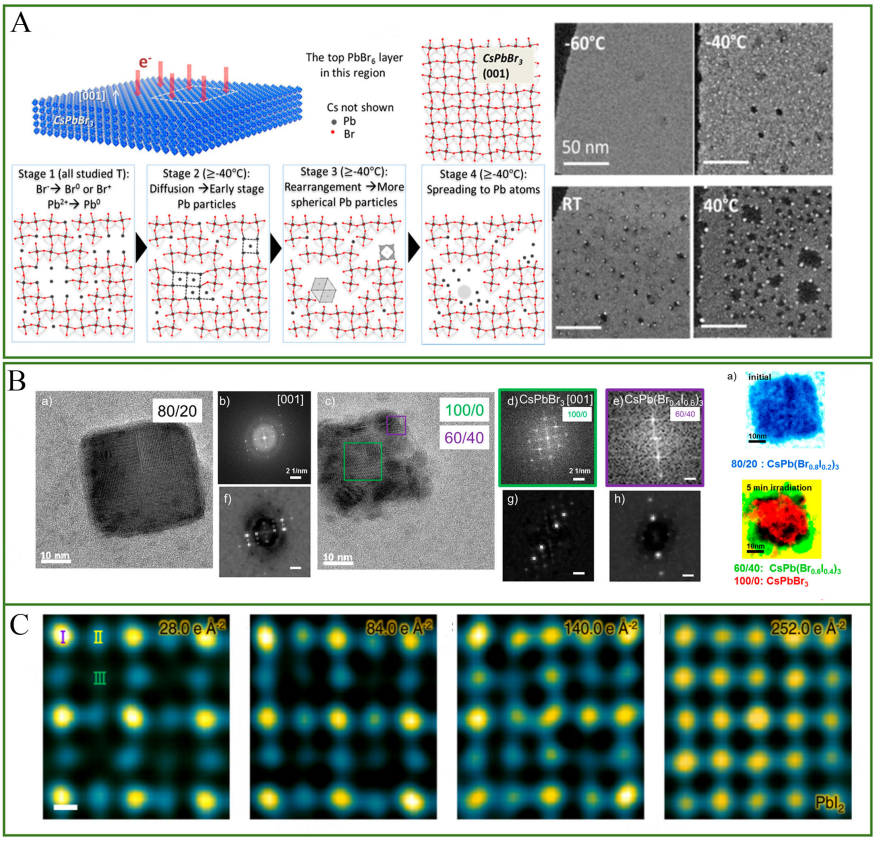

Figure 3. (A) The degradation process of $CsPbBr_3$ nanosheets when exposed to electron beam irradiation. The perspective shown is along the [001] orientation. Reproduced with the permission of Ref.[56] Copyright © 2017 American Chemical Society; (B) Phase segregation behavior of $CsPb(Br_{0.8}I_{0.2})_3$ perovskite under beam irradiation is demonstrated through the HRTEM image and the corresponding FFT pattern. After exposure to an excess electron beam dose of 1140 e $Å^{-2}$, the formation of Pb nanoparticles is observed. Reproduced with the permission of Ref.[99] Copyright © 2020 American Chemical Society; (C) HRTEM images with increased doses during the degradation into PbI_2 show the atomic scale images of the decomposition pathway. Reproduced with the permission of Ref.[39] Copyright © 2021 Springer Nature. FFT: Fast fourier transform; HRTEM :High-resolution TEM; TEM: Transmission electron microscopy.

induced by electrons. Additionally, by analyzing HRTEM and HAADF-STEM images alongside fast Fourier transform (FFT) patterns, they observed the reduction of certain Pb^{2+} ions to Pb^0, along with spontaneous migration and clustering of Pb atoms. This study offers a microscopic perspective on the degradation patterns of inorganic perovskites when subjected to extended exposure to electron beams. Moreover, it emphasizes the importance of monitoring dynamic changes in intrinsic components and local phase evolution to effectively characterize HPs in TEM, thereby providing valuable information for regulating electron beam dosage.

Funk *et al.* utilized *in situ* TEM to observe the $CsPb(Br_{0.8}I_{0.2})_3$ perovskite in real-time, verifying the presence of a diverse phase originating from electron beam irradiation[99]. HRTEM characterization revealed the formation of a more iodine-rich phase [approximately $CsPb(Br_{0.6}I_{0.4})_3$] at the periphery of the particle, whereas a central region maintained a pristine bromide phase ($CsPbBr_3$) [Figure 3B]. These findings offer valuable insights into the phase separation mechanism and have the potential to guide the development of phase-stable perovskite semiconductors.

Chen *et al.* observed a two-step decomposition pathway of $MAPbI_3$ under an ultra-low dose condition in real space at the atomic scale [Figure 3C][39]. The initial stage of decomposition involved the loss of MA^+ ions, followed by the collapse of the perovskite structure into 6H-PbI_2. Notably, an intermediate phase ($MA_{0.5}PbI_3$) with locally ordered vacancies was observed, demonstrating robust stability prior to the complete collapse of the perovskite structure. Additionally, the authors highlighted that C-N bonds could be readily disrupted upon irradiation, resulting in the release of NH_3 and HI and the formation of hydrocarbons. These results enhance the comprehension of the degradation process, offering detailed insights at the atomic level that contribute to understanding its core characteristics.

Heat

In situ heating TEM is a powerful technology in materials science allowing samples to be thermally stimulated for the study of dynamic properties such as catalysis, phase transitions, sublimation, and materials growth. Typically, *in situ* heating in TEM involves using metal resistive wires or resistive membranes deposited on SiN_x windows, which heat the sample through joule heating[100,101]. Recently, Zhao *et al.* replaced traditional metal resistive heaters with 2D graphene material, significantly enhancing the performance of the *in situ* heating chip[102]. Heat is an inevitable by-product during the operation of HP devices, whether they are solar cells or LEDs. This heat can significantly affect the crystal structure and ion migration due to the fragile ion properties of HPs, thereby accelerating the degradation process. Therefore, understanding the mechanism of thermally induced degradation is crucial for future studies and can guide efforts to improve stability.

Divitini *et al.* conducted an *in situ* TEM heating experiment on a non-encapsulated PSC with a typical device architecture [indium tin oxide (ITO)/TiO_2/$MAPbI_3$/2, 2,'7, 7'-tetrakis-(N,N',di-p-methoxyphenylamine)- 9,9'-spirobifluorene (spiro-OMeTAD)/Ag][103]. They employed HAADF-STEM imaging in combination with the associated EDX elemental map to observe real-time alterations in morphology and chemical compositions [Figure 4A]. Surprisingly, the HAADF-STEM images of the perovskite layer exhibited no changes when heated to 150 °C, even though the power conversion efficiency (PCE) of the devices had irreversibly degraded above 90 °C. The researchers attributed this degradation to the inactivity of the hole transport material (HTM). As the temperature increased, holes began to form in the region of the perovskite layer close to the interface with the electron transport layer (ETL). The primary reason for the perovskite degradation was identified as the migration of iodine and lead. Furthermore, they highlighted that the device fabricated in ambient air exhibited more severe iodine migration. This study represents one of the earliest works focused on heat-induced degradation of HP materials and provides a solid foundation for subsequent research.

Concurrently with the work by Divitini, Yang *et al.* conducted similar research[104]. As depicted in Figure 4B, when the $MAPbI_3$-based PSC device was heated for 4 h at approximately 50-60 °C, defects began to appear. This phenomenon was attributed to the migration of elements induced by thermal effects, which was expedited by the presence of Schottky or Frenkel defects in the crystal structure. Additionally, they pointed out that the oxygen tended to attack the $CH_3NH_3^+$ rather than the PbI_6 component of perovskites when exposing them to the ambient air at RT. Their work provided significant insights into preventing perovskite degradation by tailoring its molecular structure, particularly the organic moiety.

Furthermore, Kim *et al.* proposed a new degradation pathway for the $MAPbI_3$ layer. They suggested that the formation of PbI_2 grains did not result directly from the crystalline $MAPbI_3$ layer, but instead from the amorphous $MAPbI_3$ layer. This contrasts with conventional ideas that posit the formation of PbI_2 starting from the grain boundary or interface[105]. In their observation, the precipitation of the trigonal PbI_2 grains

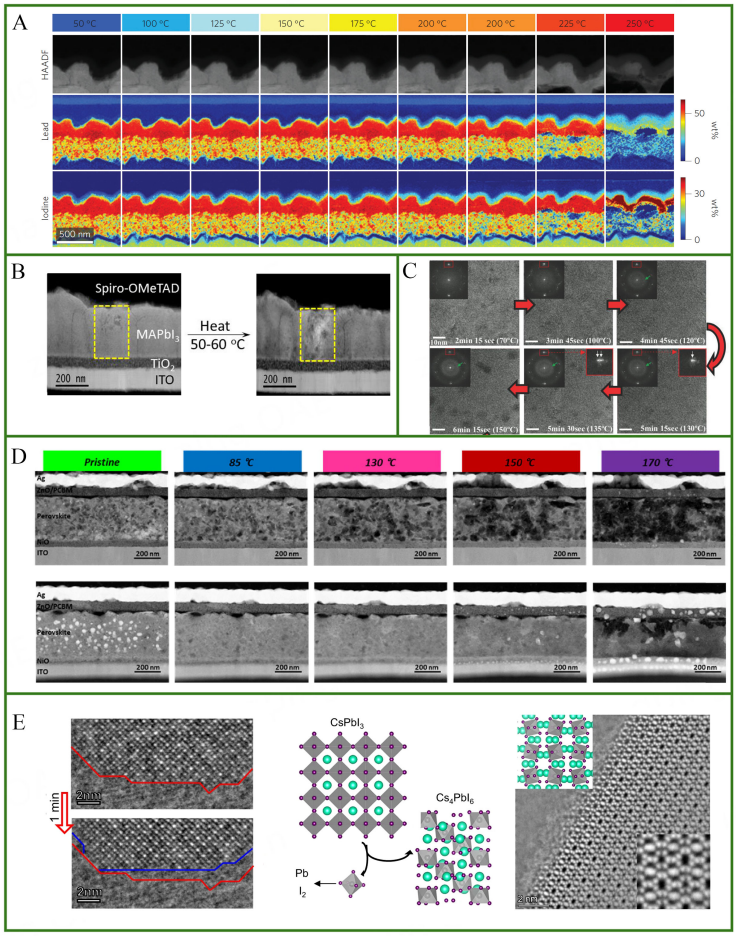

Figure 4. (A) *In situ* imaging using HAADF-STEM and characterizing with EDX reveals the variations in morphology and elemental migration of $MAPbI_3$ when exposed to rising temperatures. Reproduced with the permission of Ref.[103] Copyright © 2016 Nature Research; (B) HAADF-STEM images of a PSC undergoing thermal degradation after beam damage. Reproduced with the permission of Ref.[104] Copyright © 2016 American Chemical Society; (C) HAADF images and SAED patterns $MAPbI_3$ before and after the heat. Reproduced with the permission of Ref.[105] Copyright © 2018 WILEY VCH Verlag GmbH & Co; KGaA (D) STEM images of a PSC sample based on MA (top line) and Cs/FA/MA (bottom line), undergoing *in situ* heating from room temperature to (85, 130, 150, and 170) °C. Reproduced with the permission of Ref.[110] Copyright © Elsevier; (E) The left row shows the iDPC-STEM images demonstrating the surface degradation of a CsPbI3 nanocrystal within 1min at 200 °C. The middle row shows diagrams depicting the transformation process of $CsPbI_3$ into Pb and Cs_4PbI_6 under high-temperature conditions. The right row shows the iDPC-STEM images showing the Cs_4PbI_6 particles observed from the [211] orientation. Reproduced with the permission of Ref.[97] Copyright © 2023 Springer Nature. EDX: Energy dispersive X-ray; SAED: Selected area electron diffraction; TEM: Transmission electron microscopy; STEM: Scanning TEM; iDPC: Integrated differential phase contrast; HAADF-STEM: High angle angular dark field-scanning transmission electron microscopy.

occurred from the amorphized $MAPbI_3$ layer via an asymmetric intermediate state [Figure 4C]. This new insight contributes to a more comprehensive understanding of the degradation mechanism.

Later, Seo *et al.* noted that previous studies have primarily focused on the forward (n-i-p) device structure based on the single MA cation perovskite material. However, the MA-FA-Cs mixed cation perovskite material has shown more promise for commercialization than the single MA cation material. Additionally, the Hole transport layer (HTL) materials used in the forward structure devices, such as spiro-OMeTAD or poly[bis(4-phenyl)(2,4,6-trimethylphenyl)amine] (PTAA), commonly contain various dopants and additives. These dopants, which implicate ions that are hygroscopic and/or mobile, may negatively affect the

stability of the perovskite absorber and the device, making it challenging to identify the exact causes of perovskite degradation[106-110]. Therefore, they studied the thermally-induced effects on the photovoltaic performances of $Cs_x(FA_yMA_{1-y})_{1-x}Pb(I_zBr_{1-z})_3$ PSCs in comparison with $MAPbI_3$ PSCs, and further investigated the degradation phenomenon directly utilizing real-time *in situ* TEM[110]. They opted for the inverted (p-i-n) device structure, composed of ITO/NiO NPs/perovskite/PC61BM/ZnO NPs/Ag, to avoid the impact of the aforementioned organic HTL materials. As illustrated in Figure 4D, the perovskite device based on MA demonstrated a rapid and uninterrupted deterioration process as the temperature increased, characterized by the emergence of particles and dark voids. In contrast, the device incorporating Cs/FA/MA remained stable until it reached 130 °C, with particle formation commencing at 150 °C. However, the degradation of the Cs/FA/MA-based device intensified at 170 °C, resulting in the formation of sizable particles and voids. Common factors contributing to degradation, such as decomposed Pb and I migration, were observed in both types of PSCs. The MA-PSC displayed accelerated void formation and migration extending beyond the perovskite film as the temperature increased. Conversely, the Cs/FA/MA-PSC demonstrated negligible changes until it reached 150 °C but subsequently exhibited increased elemental migration and the emergence of large Pb-based particles and voids near the ETL side at 170 °C. The researchers attributed the deterioration to the creation of volatile cations, namely MA^+ and FA^+. They noted that the better thermal stability of FA could mitigate the deterioration of device performance. Additionally, the degradation mechanisms of these two types of devices exhibited slight variations. By analyzing EDX elemental mapping and lattice planes at the particle regions, the researchers observed the coexistence of two types of Pb and PbI_2 in the Cs/FA/MA device, while the MA-based device only exhibited PbI_2. They proposed that this phenomenon resulted from the formation of Br vacancies in the crystal structure, inducing the conversion of Pb^{2+} to Pb^0 and the subsequent formation of Pb-Pb bonds, leading to the generation of Pb particles in the Cs/FA/MA-based device. Consequently, this study offers novel insights into comprehending the degradation of perovskite materials.

Previous studies on thermally induced degradation of HPs primarily focused on morphological changes and could not achieve the atomic resolution characterization. However, with emerging low-dose technology, genuine atomic resolution imaging can now be achieved through *in situ* TEM characterization. Ma *et al.* observed the degradation process of single $CsPbI_3$ nanocrystals at the atomic scale. As shown in Figure 4E, heating the $CsPbI_3$ nanocrystals at 200 °C for 1 min caused the flat (110) surfaces in the particles to gradually disappear, exposing more (010) surfaces. With continued heating, they noted that the cubic $CsPbI_3$ nanocrystals started to deviate from their uniform structure and slowly merged into one another at temperatures over 200 °C. Combining the EDX results, they deduced that the conversion products at 300 °C may be pure Pb and Cs_4PbI_6 particles, whereas at 400 °C, only Pb is observed. Figure 4E shows the diagram of decomposition products and confirms its Cs_4PbI_6 structure. In another work, they also observed the thermal-induced degradation of $CsPbI_3$ single crystal[111]. They confirmed that thermal vibrations at high temperatures disrupted the asymmetric binding of surface ions, resulting in the extraction of these ions-either by breaking Cs-surfactant complexes or collectively pulling them out. This process initiated the degradation and fusion of $CsPbI_3$ QDs. These studies not only uncover the long-term, previously unclear dynamics of thermally induced phase transitions in HPs but also instill greater optimism and assurance for investigating further physical and chemical phenomena in HPs at the atomic scale.

Electrical bias

Electrical bias plays a crucial role in the operation of perovskite devices, where solar cells generate a built-in electric field, and LEDs are directly driven by electrical bias. Researchers apply electrical bias to samples using two primary methods. The first method involves a MEMS chip platform, where the specimen is fabricated using FIB technology and then attached to a chip installed on a specially designed holder. The source measurement unit (SMU) outside the TEM controls this setup[112]. The second approach utilizes a

micro-metal probe that makes direct contact with the sample, driven by a small piezo-driver[113]. Various studies have explored the impact of bias on HPs and devices, focusing on changes in ion migration, phase structure, morphology, and other behaviors through *in situ* TEM observation. These investigations provide valuable insights into the behavior of perovskite materials under electrical bias.

Jeangros *et al.* utilized *in situ* TEM in combination with a microchip setup to deliver a constant electrical bias to a TEM lamella of a nano solar cell[112]. The lamella consisted of active layers of $MAPbI_3$, charge carrier transport layers, and ITO and Au electrodes. Building on this foundation, they provided an *in situ* TEM observation that revealed the nanoscale degradation mechanisms of $MAPbI_3$ perovskite cells caused by bias. As shown in Figure 5A, TEM imaging and EDX analysis demonstrated that the degradation mechanisms of $MAPbI_3$ under bias were varied, primarily localized at the interface influenced by a positive bias voltage. Particularly in the context of forward conditions, iodide ions migrated toward the positively charged charge transport layer, while also evaporating alongside organic compounds within the hole transport layer. This process initiated the formation of PbI_2 NPs and empty spaces, ultimately resulting in the deterioration of the device's operational efficiency. This study provides an initial microscopic understanding of the failure mechanisms of HP devices when subjected to bias, including the development of microscopic appearance and the dynamic mechanism of ion migration. However, studies investigating atomic scale behavior in this regard are still lacking and require further advancements.

Jung *et al.* utilized *in situ* TEM to observe the oxygen diffusion process under bias, aiming to understand the degradation mechanism of HP devices[114]. Interestingly, they discovered that under forward bias, oxygen ions from the TiO_2 layers migrated into the $MAPbI_3$, causing a phase transformation from crystalline to amorphous [Figure 5B]. This severe structural change was directly attributed to the electric field-driven oxygen migration. To quantify the oxygen content, EELS measurement was conducted, revealing that 8 atomic percent (at%) of oxygen was incorporated into the $MAPbI_3$. This incorporation could potentially result in the degradation of HPs. Notably, these alterations were somewhat reversible in the absence of light and bias. However, the authors suggested that isolating the effects of moisture and oxygen alone could not fully mitigate this internally driven degradation. Overall, this study provides valuable insights into the degradation mechanism of HP devices, particularly regarding oxygen migration and TiO_2 degradation, observed through *in situ* TEM.

Kim *et al.* developed an *in situ* TEM configuration for observing the amorphization progression of HP layers when subjected to electrical bias[115]. The experimental setup [Figure 5C] enabled the researchers to observe the alterations in the structure in a nanoscale solar cell lamella subjected to a steady positive bias of 1 V. Series of TEM images captured over time vividly demonstrate the amorphization process of the HPs layers when exposed to the bias. Additionally, the morphology and phase transformation can be understood by analyzing HRTEM images and SAED patterns, which reveal the emergence of a diffuse amorphous zone. The X-ray diffraction (XRD) patterns of the perovskite materials, before and after the implementation of forward bias, further support this observation. It has been proposed that the inherent structural changes in HPs could play a role in the deterioration of device performance. Intriguingly, subjecting the samples to a temperature of 50 °C to facilitate the recrystallization process has been shown to successfully restore the lost performance. This study delves into the underlying causes of the structural instability of PSCs, particularly focusing on the fundamental mechanism of defect formation and ion migration. The observation of structural transformation at the atomic scale in real-time provides valuable insights into these factors, underscoring the considerable promise of *in situ* TEM technology in high-pressure research.

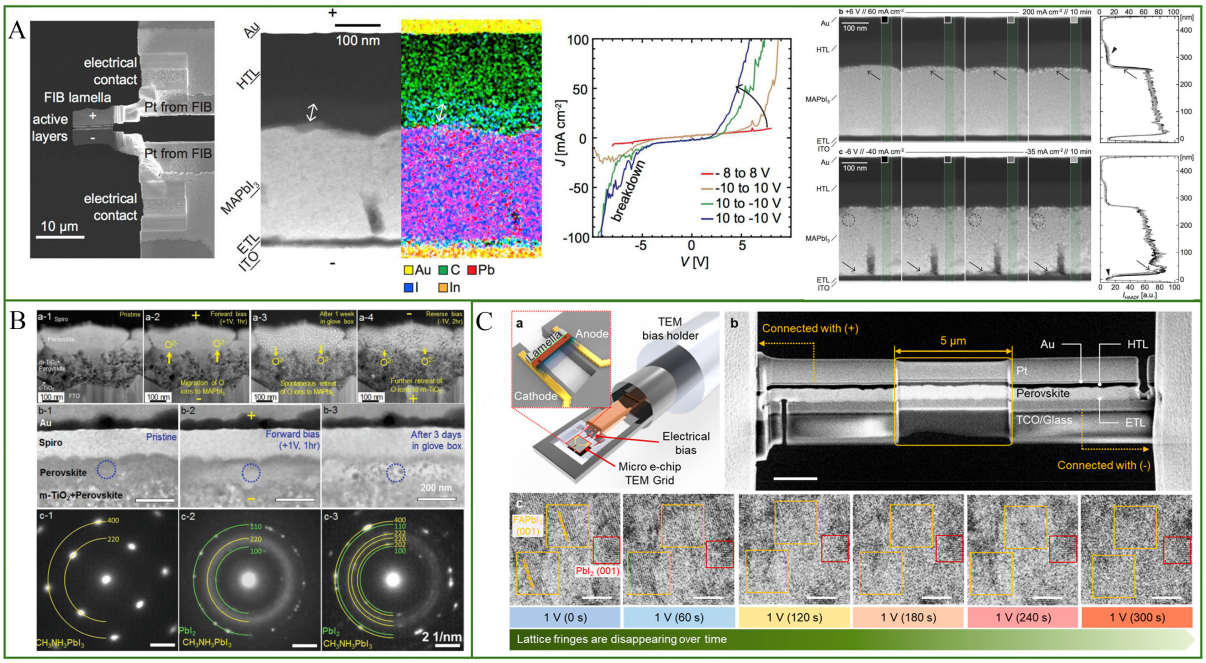

Figure 5. (A) Scanning electron microscopy (SEM) image depiction of a biasing chip connected to a TEM lamella prepared using FIB for conducting *in situ* electrical measurements. The accompanying HAADF-STEM image along with an EDX mapping showcases the initial microstructure. Acquisition of variable J-V curves through TEM observation, coupled with HAADF images, demonstrates the morphological evolution at different electrical biases. Reproduced with the permission of Ref.[112] Copyright © 2016 American Chemical Society; (B) HAADF-STEM, Bright Field TEM (BFTEM), and SAED were employed for the real-time monitoring of the morphology and structural variations of $MAPbI_3$ under *in situ* electrical bias. Reproduced with the permission of Ref.[114] Copyright © 2018 Wiley-VCH; (C) A diagram illustrating the arrangement of the *in situ* TEM sample with an applied electrical bias, accompanied by an SEM image of the nano-solar cell lamella prepared using FIB. The scale bar represents 2 μm. Sequential HRTEM images of perovskite subjected to an electrical bias of 1 V. Reproduced with the permission of Ref.[115] Copyright © 2021 American Chemical Society. EDX: Energy dispersive X-ray; TEM: Transmission electron microscopy; FIB: Focused ion beam; HRTEM :High-resolution TEM; HAADF-STEM: High angle angular dark field-scanning transmission electron microscopy.

Light

Light plays a crucial role in the operation of PSCs. Therefore, investigating changes in the morphology and structure of perovskite materials under light is a promising avenue. This approach provides a comprehensive understanding of the relationship between structure, properties, and performance, ultimately facilitating the development of light-responsive materials-based technologies. Various techniques have been proposed to incorporate light into TEM, including the use of a light path setup, a TEM-STEM probe holder, and MEMS chips[116]. The light path setup, which consists of mirrors and an optical lens, directs light onto the sample inside the TEM. However, implementing such setups requires significant modifications to the TEM system. Fortunately, advancements in MEMS technology have allowed for the integration of compact MEMS chips into the *in situ* optical TEM holder. In this configuration, the light source is positioned in front of the specimen, while the circuitry is integrated within the chips[117].

Our research group pioneered a novel on-chip technique known as light-incorporated *in situ* TEM (LI^2ST) for studying HPs at the nanoscale[118]. This method enables real-time tracking of structural transformations triggered by light at specific locations. The *in situ* platform is based on a MEMS chip, specifically designed for adjustable light illumination with customizable multi-wavelength capabilities [Figure 6A]. We fabricated perovskite samples using the thermal evaporation method. Initially, we captured SAED patterns from neighboring $CsPbBr_3$ grains, revealing the crystallographic structure in its orthorhombic form along the [112] zone axis (indicated by the white circle) without light stimulation. No significant changes were

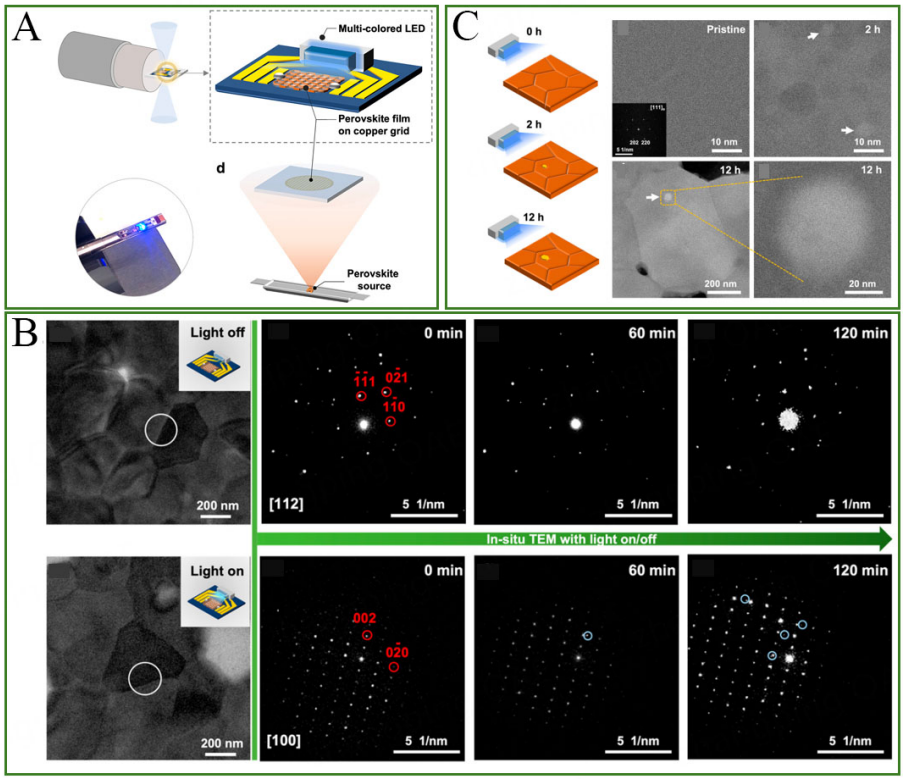

Figure 6. (A)The schematic diagram of LI^{2}ST (B) The TEM images and corresponding SAED patterns of HPs film in the light-on state and light-off state for 0, 60, and 120 min, respectively (C) HAADF-STEM images of the HP sample under different illumination times (0, 2, and 12 h) reveal the occurrence of intragrain nucleation and growth of $PbBr_2$ impurity clusters. (marked using white arrows). Reproduced with the permission of Ref.[118] Copyright © 2023 American Chemical Society. TEM: Transmission electron microscopy; SAED: Selected area electron diffraction; HPs: Halide perovskites; HAADF-STEM: High angle angular dark field-scanning transmission electron microscopy.

observed after 60 and 120 min. Subsequently, we repeated the experiment with the light turned on. The initial SAED pattern from another pair of neighboring $CsPbBr_3$ grains showed a consistent orthorhombic phase with a [100] zone axis. After 60 min of light exposure, a new diffraction spot emerged (indicated by the blue circle), and the intensity of these additional diffraction spots increased further after 120 min [Figure 6B], indicating the formation of new phases induced by the light stimulus. Our calculations suggest that the newly formed phase is $PbBr_2$. To obtain detailed atomic information and observe microstructural changes, we employed aberration-corrected STEM for *ex situ* high-resolution imaging [Figure 6C]. After two hours of light exposure, nanoclusters appeared in the HAADF-STEM image, which we attributed to $PbBr_2$ generation. Interestingly, these $PbBr_2$ nanoclusters were primarily located within the intragrain regions rather than at the grain boundaries. Extending the illumination period to 12 h resulted in significantly larger nanoclusters, suggesting that localized expansion of $PbBr_2$ nanoclusters induces perovskite degradation. Our work proposes a distinctive microstructural mechanism for HP degradation under light illumination, attributed to ion migration induced by the photo effect.

However, due to the limitations of the TEM available at that time, we could only observe changes in the material's morphology and diffraction pattern during the *in situ* experiment. Capturing the evolution process of phase transition at the atomic scale can provide us with a deeper understanding of the decomposition mechanism. Looking ahead, the integration of 4D-STEM technology could offer additional opportunities and enhanced capabilities for observing microstructural changes at the atomic scale.

Ambient atmosphere

We have mentioned that materials exhibit distinct behaviors under various atmospheric conditions compared to a high vacuum. In today's context, moisture-induced chemical degradation presents a significant challenge to the advancement of HP technology. This degradation can result in the rapid decomposition of the perovskite material, potentially leading to lead dissolution into the environment. Consequently, it is essential to conduct thorough investigations into the molecular-level stability and degradation of materials across different environmental conditions. This knowledge will play a pivotal role in developing more stable compositions and designing robust device architectures.

For the first time, the degradation mechanisms of $MAPbI_3$ under different atmospheres were investigated using *in situ* gas-cell TEM by Fan *et al.*[119]. The experimental setup maintained a controlled atmosphere of either vacuum or dry air, with a chamber pressure of 700 Torr during the control experiment. Instead of focusing on the FIB-prepared full device cross-section specimen, their attention was directed towards the atomic structural changes of the HPs, which provide deeper insights into the degradation mechanisms of perovskite materials. As shown in Figure 7A and B, traces of PbI_2 were observed after subjecting the sample to a temperature of 85 °C for 400 seconds under vacuum conditions. Similarly, Figure 7C demonstrates the same evolution pathway for $MAPbI_3$ under dry air. This evolution involved the gradual transformation of the crystalline structure of $MAPbI_3$ perovskite from tetragonal $MAPbI_3$ to trigonal PbI_2 layered crystals along a specific crystallographic direction. Consequently, the researchers concluded that thermal effects alone are responsible for the degradation of the $MAPbI_3$ perovskite in both dry air and ambient vacuum conditions. They also emphasized that surface degradation initiates crystal structure transitions through a low energy barrier pathway, implying a degradation process that occurs layer by layer, starting from the crystal surface. Additionally, they fabricated an encapsulation layer on the $MAPbI_3$ surface to suppress the layer-by-layer thermal degradation and achieved promising results. In this work, they proposed a new thermal degradation model, suggesting novel strategies for enhancing the stability of perovskite materials.

Akhavan Kazemi *et al.* investigated the degradation mechanism of $MAPbI_3$ caused by moisture using *in situ* liquid-cell TEM and *in situ* XRD techniques at 85% Relative Humidity (RH)[120]. Figure 7D provides complementary insights into the chemical transformation from $MAPbI_3$ to $MAPbI_3{\cdot}H_2O$, a finding corroborated by 2D solid-state nuclear magnetic resonance (ssNMR) measurements. The researchers highlighted that the chemical transformation from $MAPbI_3$ to $MAPbI_3{\cdot}H_2O$ occurs via a front-phase migration mechanism at the micrometer scale. The formation of PbI_2 originates from the nanoscale dissolution of $MAPbI_3{\cdot}H_2O$ and the recrystallization of larger PbI_2 particles. Initially, the PbI_2 particles nucleate and grow isotopically before forming bulgy particles. Subsequently, they grow preferentially in a specific direction, resulting in the formation of more elongated PbI_2 particles and eventually leading to dendritic growth. This study represents the first time that live observations of PSCs under humid conditions have been conducted through *in situ* liquid-cell TEM experiments, providing a real-time and clear evaluation of the reaction mechanisms at the nanoscale.

In this chapter, we summarize the applications of *in situ* TEM in studying the degradation mechanism of HPs. The first crucial consideration when investigating degradation mechanisms is to ensure that the material remains undamaged by the electron beam. Initially, researchers primarily relied on observing morphological changes, SAED patterns, and Energy dispersive X-ray spectroscopy (EDS) mapping. However, EDS mapping sometimes fails to provide useful information due to the low count rate of perovskite materials. Fortunately, advancements in low-dose technology now allow us to observe structural changes at the atomic scale *in situ*. Nevertheless, observing perovskite materials with high organic content in the A site remains challenging. High-efficiency PSCs typically contain more than 90% organic content. Additionally, the detailed degradation pathways differ significantly between inorganic and organic

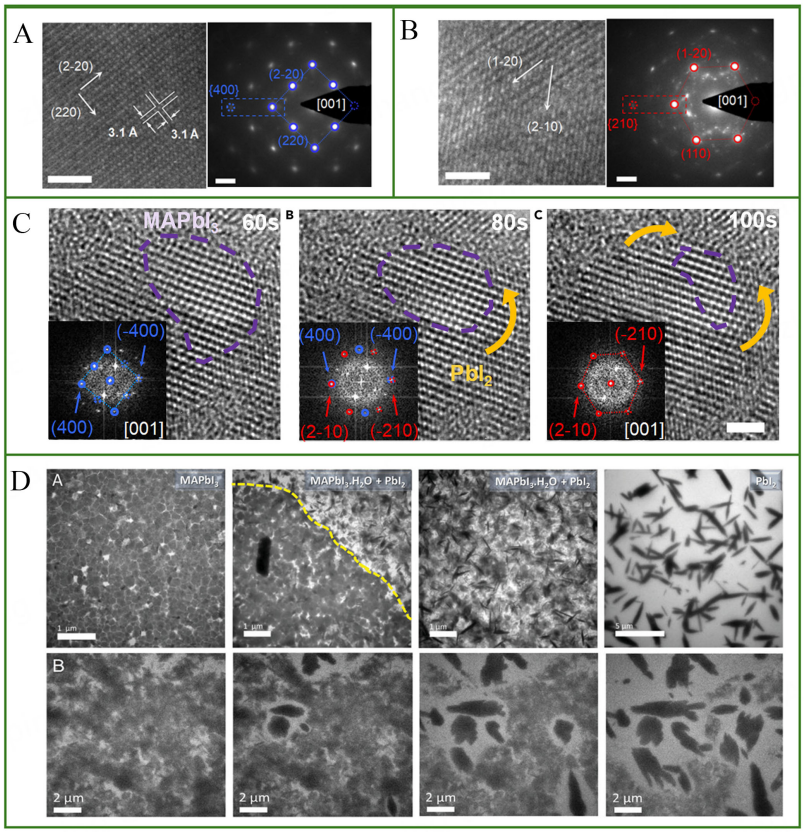

Figure 7. (A) HRTEM image and SAED pattern of $MAPbI_3$ before heating under vacuum; (B) HRTEM image and SED pattern of $MAPbI_3$ after heating at 85 °C for 400 s under vacuum; (C) HRTEM image and SED pattern of an individual $MAPbI_3$ showing the heat-induced degradation process under a dry air atmosphere. Reproduced with the permission of Ref.[119] Copyright © 2017 Elsevier; (D) *In situ* liquid-cell TEM monitoring the transformation of $MAPbI_3$ to $MAPbI_3{\cdot}H_2O$ and PbI_2 (top line), as well as the dissolution of $MAPbI_3{\cdot}H_2O$ and subsequent recrystallization into PbI_2 (bottom line). Reproduced with the permission of Ref.[120] Copyright © 2021 John Wiley & Sons. HRTEM :High-resolution TEM; TEM: Transmission electron microscopy; SAED: Selected area electron diffraction; SED: Scanning ED; ED: Electron diffraction.

perovskites. While ion substitutions in the B and X sites primarily modulate the bandgap, mixed ions in the X site may lead to phase separation[121]. However, the substitution of different organic ions in the A site significantly influences stability. Among all organic and inorganic monovalent cations, MA^+ possesses the most appropriate effective radius for achieving proper phase stability in HPs. Nonetheless, it exhibits chemical instability. Some literature suggests that MA^+ undergoes deprotonation in the presence of O_2/H_2O when leaving the crystal in the atmosphere[122-124]. Regarding FA^+, its reduced acidity, greater mass, and smaller dipole moment contribute to its superior chemical stability compared to MA^+. Consequently, $FAPbI_3$ exhibits notably enhanced thermal stability in an inert environment when contrasted with $MAPbI_3$. Additionally, Cs^+ cations exhibit even higher chemical stability than FA due to their non-volatility and resistance to deprotonation[125]. However, at RT, the cubic α-phase of $FAPbI_3$ and the orthorhombic γ-phase of $CsPbI_3$ are not thermodynamically stable; their stable forms are represented by the non-perovskite, non-photoactive δ-phases[85]. It is worth noting that to realize a better stabilization effect, some literature has reported that triple-cation recipes such as $FA_{0.79}MA_{0.16}Cs_{0.05}Pb(I_{0.83}Br_{0.17})_3$ usually show higher stability, which has been applied in recent studies[126,127]. In previous *in situ* TEM investigations of HPs, $MAPbI_3$ is the most studied material, and more research should focus on the mixed HPs system. To illustrate, when investigating perovskite degradation under various atmospheres, both articles focused on $MAPbI_3$ as the research subject. In addition, due to the low endurance of organic cations to electron beam-induced

damage, it is also important to facilitate the advancements in low-dose technologies to realize the *in situ* observations of the organic perovskites' structural evolutions without unwanted damage.

SUMMARIES AND PERSPECTIVES

In this review, we have explored the application of *in situ* TEM methodologies for studying dynamic microstructural transformations and phase transitions in HPs under diverse external stimuli. As anticipated, these techniques offer unparalleled advantages, enabling real-time imaging and spectroscopy. They allow direct monitoring of structural and chemical alterations in HPs during their operational processes. While these studies have significantly advanced our understanding of HPs, several critical challenges remain to be addressed in the future.

Firstly, the actual operational conditions of PSCs are quite complex and demanding. These cells must simultaneously withstand high temperatures, intense light, ambient atmosphere, and electrical bias. However, current research often focuses on a single stimulus in each experiment, which may not accurately reflect the true working conditions. The effects caused by each external stimulus can interact with one another, preventing us from observing the complete landscape of PSCs' operational dynamics. Therefore, there is a need to design a more realistic environment that allows us to monitor the actual working behaviors and degradation processes of PSCs. By doing so, we can gain insights into the degradation mechanisms and understand their corresponding influences on device performance. Ultimately, this knowledge will facilitate the development of high-efficiency and stable PSCs.

Secondly, TEM observations are limited to a small area of the perovskite material and must account for the effects of ED, which can sometimes lead to misleading conclusions. For instance, some researchers have noted that SAED and HRTEM results initially misidentify PbI_2 as perovskite structures during the characterization of HPs[128,129]. Besides, although TEM can provide an in-depth understanding of structural and chemical information, it falls short in determining the photo-related physical properties that are crucial to the performances of HPs. To address this, it is advisable to complement TEM with other *in situ* characterization methods, ensuring more reliable and comprehensive results[130,131]. By combining *in situ* TEM with techniques such as *in situ* atomic force microscopy (AFM), Kelvin probe force microscopy (KPFM), and other probing methods, researchers can gain valuable insights into structural, morphological, and electronic property changes during degradation processes[132]. Such information is not accessible through *in situ* TEM alone. Additionally, integrating *in situ* TEM with *in situ* SEM-cathodoluminescence (SEM-CL) allows for the characterization of structures and morphologies at various scales, along with variations in cathodoluminescence to reveal the evolutions of defects and band structures[133]. Furthermore, by combining *in situ* TEM with *in situ* infrared spectroscopy and other optoelectronic tests, researchers can understand how structural changes impact device performance[134]. Looking ahead, a focus on combining multiple techniques to obtain multi-scale, multi-type high-throughput data will be enlightening for advancing our understanding of perovskite stability.

Thirdly, the application of *in situ* TEM imaging to HPs is currently in its initial phase, primarily focusing on characterizing the relatively large-scale structure. However, there remains a clear gap in research concerning the fundamental microscopic structures that significantly influence the inherent physicochemical characteristics of HPs. These structures include grain boundaries, imperfections within the grains, and atomic-level surfaces/interfaces observed in real-time. It is crucial to unravel the intricate details of these microstructures using high-resolution (S/TEM) techniques, which offer superior spatial, temporal, and energy capabilities. This understanding plays a pivotal role in deciphering their cumulative impact on optoelectronic properties, ultimately unlocking the full potential of HPs by considering their structure,

properties, and performance.

Fortunately, several exciting new technologies have been introduced in today's TEM characterization, including iDPC, 4D-STEM, and ptychography. Integrating these novel techniques with *in situ* TEM characterization offers us greater opportunities and capabilities to observe microstructural changes at the atomic scale. iDPC is an emerging STEM technique used to generate potential maps of samples. It has found applications in characterizing the atomic structures of electron beam-sensitive materials, such as porous zeolites, organic-inorganic hybrid perovskites, and metal-organic frameworks[43,135-138]. In addition, 4D-STEM is a powerful analysis method that relies on an advanced high-speed pixel array detector to record a 4D dataset[44]. This dataset includes 2D images and 2D diffraction patterns at each scanning pixel, containing nearly all relevant information about the samples[139,140]. By adding virtual detectors, 4D-STEM can reconstruct traditional images such as HAADF-STEM images and extract phase information to reconstruct the electrostatic potential of the specimen[141-144]. When combined with *in situ* characterization, 4D-STEM enables real-time, atomic-level observation of phase transitions, structural changes, and physical responses, providing valuable insights for optimizing these materials across various applications[145]. Moreover, ptychography is another emerging computational method that extracts quantitative object functions from a series of convergent-beam ED patterns using local overlapped probes[146,147]. It can be conducted with a defocused probe for high dose efficiency, particularly advantageous for imaging beam-sensitive materials. Moreover, ptychography surpasses the resolution limit of traditional aperture and eliminates aberrations. Images reconstructed from an iterative ptychographic algorithm achieve spatial resolutions down to 23 picometers, allowing precise measurements of structural details even at limited doses[148,149]. This capability holds promise for time-resolved *in situ* characterization, often accompanied by high dose consumption. To facilitate the combination of these advanced imaging and analysis approaches with *in situ* S/TEM observations, the advantages of ultra-high speed, high quantum efficiency, and high SNR detectors are becoming increasingly important.

DECLARATIONS

Authors' contributions

Summarized and wrote the original draft: Hao, L.
Made substantial contributions to the conception and design of the review: Cai, S.

Availability of data and materials

Not applicable.

Financial support and sponsorship

This research was supported by the Startup Grant from The Hong Kong Polytechnic University (1-BDCM), the General Research Fund (Nos. 15306021 and 15306122), and the Early Career Scheme (No. 25305023), all provided by The Hong Kong Research Grants Council (RGC).

Conflicts of interest

All authors declared that there are no conflicts of interest.

Ethical approval and consent to participate

Not applicable.

Consent for publication

Not applicable.

REFERENCES

1. Dong, H.; Ran, C.; Gao, W.; Li, M.; Xia, Y.; Huang, W. Metal halide perovskite for next-generation optoelectronics: progresses and prospects. *eLight* **2023**, *3*, 3. DOI
2. Zhao, Y.; Zhu, K. Organic-inorganic hybrid lead halide perovskites for optoelectronic and electronic applications. *Chem. Soc. Rev.* **2016**, *45*, 655-89. DOI
3. Huang, J.; Yuan, Y.; Shao, Y.; Yan, Y. Understanding the physical properties of hybrid perovskites for photovoltaic applications. *Nat. Rev. Mater.* **2017**, *2*, 1-19. DOI
4. Jiang, Q.; Zhao, Y.; Zhang, X.; et al. Surface passivation of perovskite film for efficient solar cells. *Nat. Photonics.* **2019**, *13*, 460-6. DOI
5. Lin, Y.; Lin, G.; Sun, B.; Guo, X. Nanocrystalline perovskite hybrid photodetectors with high performance in almost every figure of merit. *Adv. Funct. Mater.* **2018**, *28*, 1705589. DOI
6. Chen, P.; Ong, W.; Shi, Z.; Zhao, X.; Li, N. Pb-based halide perovskites: recent advances in photo(electro)catalytic applications and looking beyond. *Adv. Funct. Mater.* **2020**, *30*, 1909667. DOI
7. Ran, J.; Dyck, O.; Wang, X.; Yang, B.; Geohegan, D. B.; Xiao, K. Electron-beam-related studies of halide perovskites: challenges and opportunities. *Adv. Energy. Mater.* **2020**, *10*, 1903191. DOI
8. Liu, D.; Guo, Y.; Que, M.; et al. Metal halide perovskite nanocrystals: application in high-performance photodetectors. *Mater. Adv.* **2021**, *2*, 856-79. DOI
9. Yuan, M.; Quan, L. N.; Comin, R.; et al. Perovskite energy funnels for efficient light-emitting diodes. *Nat. Nanotechnol.* **2016**, *11*, 872-7. DOI
10. Zhao, Y.; Ma, F.; Qu, Z.; et al. Inactive $(PbI_2)_2RbCl$ stabilizes perovskite films for efficient solar cells. *Science* **2022**, *377*, 531-4. DOI
11. Dou, L.; Yang, Y. M.; You, J.; et al. Solution-processed hybrid perovskite photodetectors with high detectivity. *Nat. Commun.* **2014**, *5*, 5404. DOI
12. Wang, H.; Kim, D. H. Perovskite-based photodetectors: materials and devices. *Chem. Soc. Rev.* **2017**, *46*, 5204-36. DOI
13. Li, Z.; Hong, E.; Zhang, X.; Deng, M.; Fang, X. Perovskite-type 2D materials for high-performance photodetectors. *J. Phys. Chem. Lett.* **2022**, *13*, 1215-25. DOI
14. Kojima, A.; Teshima, K.; Shirai, Y.; Miyasaka, T. Organometal halide perovskites as visible-light sensitizers for photovoltaic cells. *J. Am. Chem. Soc.* **2009**, *131*, 6050-1. DOI
15. Min, H.; Lee, D. Y.; Kim, J.; et al. Perovskite solar cells with atomically coherent interlayers on SnO_2 electrodes. *Nature* **2021**, *598*, 444-50. DOI
16. Best research-cell efficiency chart. Available from: https://www.nrel.gov/pv/cell-efficiency.html. [Last accessed on 21 Jan 2025].
17. Hassan, Y.; Park, J. H.; Crawford, M. L.; et al. Ligand-engineered bandgap stability in mixed-halide perovskite LEDs. *Nature* **2021**, *591*, 72-7. DOI
18. Ma, D.; Lin, K.; Dong, Y.; et al. Distribution control enables efficient reduced-dimensional perovskite LEDs. *Nature* **2021**, *599*, 594-8. DOI
19. Lin, K.; Xing, J.; Quan, L. N.; et al. Perovskite light-emitting diodes with external quantum efficiency exceeding 20 per cent. *Nature* **2018**, *562*, 245-8. DOI
20. Wei, Y.; Cheng, Z.; Lin, J. An overview on enhancing the stability of lead halide perovskite quantum dots and their applications in phosphor-converted LEDs. *Chem. Soc. Rev.* **2019**, *48*, 310-50. DOI
21. Xiao, Z.; Yan, Y. Progress in theoretical study of metal halide perovskite solar cell materials. *Adv. Energy. Mater.* **2017**, *7*, 1701136. DOI
22. Kieslich, G.; Sun, S.; Cheetham, A. K. Solid-state principles applied to organic-inorganic perovskites: new tricks for an old dog. *Chem. Sci.* **2014**, *5*, 4712-5. DOI
23. Kieslich, G.; Sun, S.; Cheetham, A. K. An extended tolerance factor approach for organic-inorganic perovskites. *Chem. Sci.* **2015**, *6*, 3430-3. DOI PubMed PMC
24. Bartel, C. J.; Sutton, C.; Goldsmith, B. R.; et al. New tolerance factor to predict the stability of perovskite oxides and halides. *Sci. Adv.* **2019**, *5*, eaav0693. DOI PubMed PMC
25. Trizio L, Infante I, Abdelhady AL, Brovelli S, Manna L. Guidelines for the characterization of metal halide nanocrystals. *Trends. Chem.* **2021**, *3*, 631-44. DOI
26. Si, H.; Zhang, S.; Ma, S.; et al. Emerging conductive atomic force microscopy for metal halide perovskite materials and solar cells. *Adv. Energy. Mater.* **2020**, *10*, 1903922. DOI
27. Qin, M.; Chan, P. F.; Lu, X. A Systematic review of metal halide perovskite crystallization and film formation mechanism unveiled by in situ GIWAXS. *Adv. Mater.* **2021**, *33*, e2105290. DOI
28. Song, K.; Liu, L.; Zhang, D.; Hautzinger, M. P.; Jin, S.; Han, Y. Atomic-resolution imaging of halide perovskites using electron microscopy. *Adv. Energy. Mater.* **2020**, *10*, 1904006. DOI

29. Kirchartz, T.; Márquez, J. A.; Stolterfoht, M.; Unold, T. Photoluminescence-based characterization of halide perovskites for photovoltaics. *Adv. Energy. Mater.* **2020**, *10*, 1904134. DOI
30. Zai, H.; Ma, Y.; Chen, Q.; Zhou, H. Ion migration in halide perovskite solar cells: mechanism, characterization, impact and suppression. *J. Energy. Chem.* **2021**, *63*, 528-49. DOI
31. Duong, T.; Mulmudi, H. K.; Shen, H.; et al. Structural engineering using rubidium iodide as a dopant under excess lead iodide conditions for high efficiency and stable perovskites. *Nano. Energy.* **2016**, *30*, 330-40. DOI
32. Ran, C.; Xu, J.; Gao, W.; Huang, C.; Dou, S. Defects in metal triiodide perovskite materials towards high-performance solar cells: origin, impact, characterization, and engineering. *Chem. Soc. Rev.* **2018**, *47*, 4581-610. DOI PubMed
33. Chen, B.; Rudd, P. N.; Yang, S.; Yuan, Y.; Huang, J. Imperfections and their passivation in halide perovskite solar cells. *Chem. Soc. Rev.* **2019**, *48*, 3842-67. DOI
34. Haider, M.; Uhlemann, S.; Schwan, E.; Rose, H.; Kabius, B.; Urban, K. Electron microscopy image enhanced. *Nature* **1998**, *392*, 768-9. DOI
35. Muller, D. A. Structure and bonding at the atomic scale by scanning transmission electron microscopy. *Nat. Mater.* **2009**, *8*, 263-70. DOI PubMed
36. Qi, R.; Li, N.; Du, J.; et al. Four-dimensional vibrational spectroscopy for nanoscale mapping of phonon dispersion in BN nanotubes. *Nat. Commun.* **2021**, *12*, 1179. DOI PubMed PMC
37. Yan, X.; Liu, C.; Gadre, C. A.; et al. Single-defect phonons imaged by electron microscopy. *Nature* **2021**, *589*, 65-9. DOI
38. Yao, L.; Xia, W.; Zhang, H.; et al. *In situ* visualization of sodium transport and conversion reactions of FeS_2 nanotubes made by morphology engineering. *Nano. Energy.* **2019**, *60*, 424-31. DOI
39. Chen, S.; Wu, C.; Han, B.; et al. Atomic-scale imaging of $CH_3NH_3PbI_3$ structure and its decomposition pathway. *Nat. Commun.* **2021**, *12*, 5516. DOI PubMed PMC
40. Zhang, D.; Zhu, Y.; Liu, L.; et al. Atomic-resolution transmission electron microscopy of electron beam-sensitive crystalline materials. *Science* **2018**, *359*, 675-9. DOI
41. Levin, B. D. A. Direct detectors and their applications in electron microscopy for materials science. *J. Phys. Mater.* **2021**, *4*, 042005. DOI
42. Roberts, P.; Chapman, J.; Macleod, A. A CCD-based image recording system for the CTEM. *Ultramicroscopy* **1982**, *8*, 385-96. DOI
43. Lazić, I.; Bosch, E. G. T.; Lazar, S. Phase contrast STEM for thin samples: integrated differential phase contrast. *Ultramicroscopy* **2016**, *160*, 265-80. DOI PubMed
44. Ophus, C. Four-dimensional scanning transmission electron microscopy (4D-STEM): from scanning nanodiffraction to ptychography and beyond. *Microsc. Microanal.* **2019**, *25*, 563-82. DOI PubMed
45. Xiao, C.; Li, Z.; Guthrey, H.; et al. Mechanisms of electron-beam-induced damage in perovskite thin films revealed by cathodoluminescence spectroscopy. *J. Phys. Chem. C.* **2015**, *119*, 26904-11. DOI
46. Cai, Z.; Wu, Y.; Chen, S. Energy-dependent knock-on damage of organic-inorganic hybrid perovskites under electron beam irradiation: first-principles insights. *Appl. Phys. Lett.* **2021**, *119*, 123901. DOI
47. Liu, W.; Zheng, J.; Shang, M.; et al. Electron-beam irradiation-hard metal-halide perovskite nanocrystals. *J. Mater. Chem. A.* **2019**, *7*, 10912-7. DOI
48. Rothmann, M. U.; Li, W.; Zhu, Y.; et al. Structural and chemical changes to $CH_3NH_3PbI_3$ induced by electron and gallium ion beams. *Adv. Mater.* **2018**, *30*, e1800629. DOI
49. Cai, S.; Li, Z.; Zhang, Y.; et al. Intragrain impurity annihilation for highly efficient and stable perovskite solar cells. *Nat. Commun.* **2024**, *15*, 2329. DOI PubMed PMC
50. Rothmann, M. U.; Li, W.; Zhu, Y.; et al. Direct observation of intrinsic twin domains in tetragonal $CH_3NH_3PbI_3$. *Nat. Commun.* **2017**, *8*, 14547. DOI PubMed PMC
51. Chen, S.; Zhang, Y.; Zhang, X.; et al. General decomposition pathway of organic-inorganic hybrid perovskites through an intermediate superstructure and its suppression mechanism. *Adv. Mater.* **2020**, *32*, e2001107. DOI
52. Chen, S.; Zhang, Y.; Zhao, J.; et al. Transmission electron microscopy of organic-inorganic hybrid perovskites: myths and truths. *Sci. Bull. (Beijing).* **2020**, *65*, 1643-9. DOI
53. Li, Y.; Zhou, W.; Li, Y.; et al. Unravelling atomic structure and degradation mechanisms of organic-inorganic halide perovskites by cryo-EM. *Joule* **2019**, *3*, 2854-66. DOI
54. Zhu, Y.; Gui, Z.; Wang, Q.; et al. Direct atomic scale characterization of the surface structure and planar defects in the organic-inorganic hybrid $CH_3NH_3PbI_3$ by cryo-TEM. *Nano. Energy.* **2020**, *73*, 104820. DOI
55. Aguiar, J. A.; Wozny, S.; Holesinger, T. G.; et al. *In situ* investigation of the formation and metastability of formamidinium lead tri-iodide perovskite solar cells. *Energy. Environ. Sci.* **2016**, *9*, 2372-82. DOI
56. Dang, Z.; Shamsi, J.; Palazon, F.; et al. *In situ* transmission electron microscopy study of electron beam-induced transformations in colloidal cesium lead halide perovskite nanocrystals. *ACS. Nano.* **2017**, *11*, 2124-32. DOI
57. Chen, S.; Zhang, X.; Zhao, J.; et al. Atomic scale insights into structure instability and decomposition pathway of methylammonium lead iodide perovskite. *Nat. Commun.* **2018**, *9*, 4807. DOI PubMed PMC
58. Doherty, T. A. S.; Nagane, S.; Kubicki, D. J.; et al. Stabilized tilted-octahedra halide perovskites inhibit local formation of performance-limiting phases. *Science* **2021**, *374*, 1598-605. DOI
59. Rothmann, M. U.; Kim, J. S.; Borchert, J.; et al. Atomic-scale microstructure of metal halide perovskite. *Science* **2020**, *370*,

eabb5940. DOI
60. Ning, Z.; Gong, X.; Comin, R.; et al. Quantum-dot-in-perovskite solids. *Nature* **2015**, *523*, 324-8. DOI
61. Jung, H. J.; Stompus, C. C.; Kanatzidis, M. G.; Dravid, V. P. Self-passivation of 2D ruddlesden-popper perovskite by polytypic surface PbI_2 encapsulation. *Nano. Lett.* **2019**, *19*, 6109-17. DOI PubMed
62. Gao, G.; Xi, Q.; Zhou, H.; et al. Novel inorganic perovskite quantum dots for photocatalysis. *Nanoscale* **2017**, *9*, 12032-8. DOI
63. Wang, D.; Wu, D.; Dong, D.; et al. Polarized emission from $CsPbX_3$ perovskite quantum dots. *Nanoscale* **2016**, *8*, 11565-70. DOI
64. Guo, S.; Zhang, X.; Hao, M.; et al. Liquid-phase transfer of organic–inorganic halide perovskite films for TEM investigation and planar heterojunction fabrication. *Adv. Opt. Mater.* **2024**, *12*, 2301255. DOI
65. Lyu, B.; Li, D.; Wang, Q.; et al. Pattern-matched polymer ligands toward near-perfect synergistic passivation for high-performance and stable Br/Cl mixed perovskite light-emitting diodes. *Angew. Chem. Int. Ed.* **2024**, *63*, e202408726. DOI
66. Chen, F.; Dai, X.; Yao, K.; et al. Homogeneous mono-layer mixed-halide perovskite quantum dots towards blue light-emitting diodes with stable spectra under continuous driving. *Chem. Eng. J.* **2024**, *486*, 150435. DOI
67. Otero-Martínez, C.; Zaffalon, M. L.; Ivanov, Y. P.; et al. Ultrasmall $CsPbBr_3$ blue emissive perovskite quantum dots using K-alloyed Cs_4PbBr_6 nanocrystals as precursors. *ACS. Energy. Lett.* **2024**, *9*, 2367-77. DOI
68. Zhou, Y.; Sternlicht, H.; Padture, N. P. Transmission electron microscopy of halide perovskite materials and devices. *Joule* **2019**, *3*, 641-61. DOI
69. Kosasih, F. U.; Ducati, C. Characterising degradation of perovskite solar cells through in-situ and operando electron microscopy. *Nano. Energy.* **2018**, *47*, 243-56. DOI
70. Yao, L.; Tian, L.; Zhang, S.; et al. Low-dose transmission electron microscopy study on halide perovskites: application and challenges. *EnergyChem* **2023**, *5*, 100105. DOI
71. Han, Y.; Wang, L.; Cao, K.; et al. *In situ* TEM characterization and modulation for phase engineering of nanomaterials. *Chem. Rev.* **2023**, *123*, 14119-84. DOI
72. Sharma, R. An environmental transmission electron microscope for in situ synthesis and characterization of nanomaterials. *J. Mater. Res.* **2005**, *20*, 1695-707. DOI
73. Jinschek, J. R. Advances in the environmental transmission electron microscope (ETEM) for nanoscale *in situ* studies of gas-solid interactions. *Chem. Commun.* **2014**, *50*, 2696-706. DOI PubMed
74. Allen, J. J. Micro electro mechanical system design. 1th ed. CRC Press; 2005. p. 496. Available from: https://doi.org/10.1201/9781420027754. [Last accessed on 22 Jan 2025].
75. Alfarano, G. Eco-energy of subtle design. In: Gambardella, C.; editors. For nature/with nature: new sustainable design scenarios. Springer series in design and innovation. Springer, Cham; 2024. pp. 105-23. Available from: https://doi.org/10.1007/978-3-031-53122-4_8. [Last accessed on 22 Jan 2025].
76. Fan, Z.; Zhang, L.; Baumann, D.; et al. In situ transmission electron microscopy for energy materials and devices. *Adv. Mater.* **2019**, *31*, e1900608. DOI
77. Song, Z.; Xie, Z. H. A literature review of in situ transmission electron microscopy technique in corrosion studies. *Micron* **2018**, *112*, 69-83. DOI PubMed
78. Grancini, G.; Marras, S.; Prato, M.; et al. The impact of the crystallization processes on the structural and optical properties of hybrid perovskite films for photovoltaics. *J. Phys. Chem. Lett.* **2014**, *5*, 3836-42. DOI
79. Yang, S.; Duan, Y.; Liu, Z.; Liu, S. Recent advances in $CsPbX_3$ perovskite solar cells: focus on crystallization characteristics and controlling strategies. *Adv. Energy. Mater.* **2023**, *13*, 2201733. DOI
80. Xie, Y.; Xue, Q.; Yip, H. Metal-halide perovskite crystallization kinetics: a review of experimental and theoretical studies. *Adv. Energy. Mater.* **2021**, *11*, 2100784. DOI
81. Kim, B. H.; Yang, J.; Lee, D.; Choi, B. K.; Hyeon, T.; Park, J. Liquid-phase transmission electron microscopy for studying colloidal inorganic nanoparticles. *Adv. Mater.* **2018**, *30*, 1703316. DOI
82. Yuan, W.; Fang, K.; You, R.; Zhang, Z.; Wang, Y. Toward in situ atomistic design of catalytic active sites via controlled atmosphere transmission electron microscopy. *Acc. Mater. Res.* **2023**, *4*, 275-86. DOI
83. Tang, M.; Yuan, W.; Ou, Y.; et al. Recent progresses on structural reconstruction of nanosized metal catalysts via controlled-atmosphere transmission electron microscopy: a review. *ACS. Catal.* **2020**, *10*, 14419-50. DOI
84. Fang, K.; Yuan, W.; Wagner, J. B.; Zhang, Z.; Wang, Y. In-situ gas transmission electron microscopy. In: Sun, L.; Xu, T.; Zhang, Z.; editors. In-situ transmission electron microscopy. Singapore: Springer Nature; 2023. pp. 251-325. DOI
85. Stoumpos, C. C.; Malliakas, C. D.; Kanatzidis, M. G. Semiconducting tin and lead iodide perovskites with organic cations: phase transitions, high mobilities, and near-infrared photoluminescent properties. *Inorg. Chem.* **2013**, *52*, 9019-38. DOI
86. Qin, F.; Wang, Z.; Wang, Z. L. Anomalous growth and coalescence dynamics of hybrid perovskite nanoparticles observed by liquid-cell transmission electron microscopy. *ACS. Nano.* **2016**, *10*, 9787-93. DOI PubMed
87. Lifshitz, I.; Slyozov, V. The kinetics of precipitation from supersaturated solid solutions. *J. Phys. Chem. Solids.* **1961**, *19*, 35-50. DOI
88. Wagner, C. Theorie der alterung von niederschlägen durch umlösen (ostwald-reifung). *Z. Elektrochemie,. Ber. Bunsenges. phys. Chemie.* **1961**, *65*, 581-91. DOI
89. Viswanatha, R.; Santra, P. K.; Dasgupta, C.; Sarma, D. D. Growth mechanism of nanocrystals in solution: ZnO, a case study. *Phys. Rev. Lett.* **2007**, *98*, 255501. DOI PubMed

90. Aguiar, J. A.; Wozny, S.; Alkurd, N. R.; et al. Effect of water vapor, temperature, and rapid annealing on formamidinium lead triiodide perovskite crystallization. *ACS. Energy. Lett.* **2016**, *1*, 155-61. DOI
91. Wang, W.; Ghosh, T.; Yan, H.; et al. The growth dynamics of organic-inorganic metal halide perovskite films. *J. Am. Chem. Soc.* **2022**, *144*, 17848-56. DOI
92. Zhang, X.; Wang, F.; Zhang, B.; Zha, G.; Jie, W. Ferroelastic domains in a $CsPbBr_3$ single crystal and their phase transition characteristics: an *in situ* TEM study. *Cryst. Growth. Des.* **2020**, *20*, 4585-92. DOI
93. Gu, J.; Wu, J.; Jin, C.; et al. Solvent engineering for high conversion yields of layered raw materials into large-scale freestanding hybrid perovskite nanowires. *Nanoscale* **2018**, *10*, 17722-9. DOI
94. Ren, Y.; Liu, S.; Duan, B.; et al. Controllable intermediates by molecular self-assembly for optimizing the fabrication of large-grain perovskite films via one-step spin-coating. *J. Alloys. Compd.* **2017**, *705*, 205-10. DOI
95. Munir, R.; Sheikh, A. D.; Abdelsamie, M.; et al. Hybrid perovskite thin-film photovoltaics: in situ diagnostics and importance of the precursor solvate phases. *Adv. Mater.* **2017**, *29*, 1604113. DOI
96. Sidhoum, C.; Constantin, D.; Ihiawakrim, D.; et al. Shedding light on the birth of hybrid perovskites: a correlative study by *in situ* electron microscopy and synchrotron-based X-ray scattering. *Chem. Mater.* **2023**, *35*, 7943-56. DOI
97. Ma, M.; Zhang, X.; Chen, X.; et al. In situ imaging of the atomic phase transition dynamics in metal halide perovskites. *Nat. Commun.* **2023**, *14*, 7142. DOI PubMed PMC
98. Wu, X.; Ke, X.; Sui, M. Recent progress on advanced transmission electron microscopy characterization for halide perovskite semiconductors. *J. Semicond.* **2022**, *43*, 041106. DOI
99. Funk, H.; Shargaieva, O.; Eljarrat, A.; Unger, E. L.; Koch, C. T.; Abou-Ras, D. In situ TEM monitoring of phase-segregation in inorganic mixed halide perovskite. *J. Phys. Chem. Lett.* **2020**, *11*, 4945-50. DOI PubMed
100. Saka, H.; Kamino, T.; Ara, S.; Sasaki, K. *In situ* heating transmission electron microscopy. *MRS. Bull.* **2008**, *33*, 93-100. DOI
101. Ross, F. M. In situ transmission electron microscopy. In: Hawkes, P. W.; Spence, J. C. H.; editors. Science of microscopy. New York: Springer; 2007. pp. 445-534. DOI
102. Zhao, J.; Liang, L.; Tang, S.; et al. Graphene microheater chips for *in situ* TEM. *Nano. Lett.* **2023**, *23*, 726-34. DOI
103. Divitini, G.; Cacovich, S.; Matteocci, F.; Cinà, L.; Di, C. A.; Ducati, C. *In situ* observation of heat-induced degradation of perovskite solar cells. *Nat. Energy.* **2016**, *1*, 1-6. DOI
104. Yang, B.; Dyck, O.; Ming, W.; et al. Observation of nanoscale morphological and structural degradation in perovskite solar cells by in situ TEM. *ACS. Appl. Mater. Interfaces.* **2016**, *8*, 32333-40. DOI
105. Kim, T. W.; Shibayama, N.; Cojocaru, L.; Uchida, S.; Kondo, T.; Segawa, H. Real-time in situ observation of microstructural change in organometal halide perovskite induced by thermal degradation. *Adv. Funct. Materials.* **2018**, *28*, 1804039. DOI
106. Rombach, F. M.; Haque, S. A.; Macdonald, T. J. Lessons learned from spiro-OMeTAD and PTAA in perovskite solar cells. *Energy. Environ. Sci.* **2021**, *14*, 5161-90. DOI
107. Ren, G.; Han, W.; Deng, Y.; et al. Strategies of modifying spiro-OMeTAD materials for perovskite solar cells: a review. *J. Mater. Chem. A.* **2021**, *9*, 4589-625. DOI
108. Tumen-ulzii, G.; Qin, C.; Matsushima, T.; et al. Understanding the degradation of spiro-OMeTAD-based perovskite solar cells at high temperature. *Solar. RRL.* **2020**, *4*, 2000305. DOI
109. Wang, Y.; Duan, L.; Zhang, M.; et al. PTAA as efficient hole transport materials in perovskite solar cells: a review. *Solar. RRL.* **2022**, *6*, 2200234. DOI
110. Seo, Y.; Kim, J. H.; Kim, D.; Chung, H.; Na, S. *In situ* TEM observation of the heat-induced degradation of single- and triple-cation planar perovskite solar cells. *Nano. Energy.* **2020**, *77*, 105164. DOI
111. Ma, M.; Zhang, X.; Xu, L.; et al. Atomically unraveling the structural evolution of surfaces and interfaces in metal halide perovskite quantum dots. *Adv. Mater.* **2023**, *35*, e2300653. DOI
112. Jeangros, Q.; Duchamp, M.; Werner, J.; et al. In situ TEM analysis of organic-inorganic metal-halide perovskite solar cells under electrical bias. *Nano. Lett.* **2016**, *16*, 7013-8. DOI
113. Zheng, F.; Caron, J.; Migunov, V.; Beleggia, M.; Pozzi, G.; Dunin-borkowski, R. E. Measurement of charge density in nanoscale materials using off-axis electron holography. *J. Electron. Spectrosc. Relat. Phenom.* **2020**, *241*, 146881. DOI
114. Jung, H. J.; Kim, D.; Kim, S.; Park, J.; Dravid, V. P.; Shin, B. Stability of halide perovskite solar cell devices: in situ observation of oxygen diffusion under biasing. *Adv. Mater.* **2018**, *30*, e1802769. DOI
115. Kim, M.; Ahn, N.; Cheng, D.; et al. Imaging real-time amorphization of hybrid perovskite solar cells under electrical biasing. *ACS. Energy. Lett.* **2021**, *6*, 3530-7. DOI
116. Żak, A. M. Light-induced in situ transmission electron microscopy-development, challenges, and perspectives. *Nano. Lett.* **2022**, *22*, 9219-26. DOI PubMed PMC
117. Cai, S.; Gu, C.; Wei, Y.; Gu, M.; Pan, X.; Wang, P. Development of *in situ* optical-electrical MEMS platform for semiconductor characterization. *Ultramicroscopy* **2018**, *194*, 57-63. DOI
118. Duan, T.; Wang, W.; Cai, S.; Zhou, Y. On-chip light-incorporated *in situ* transmission electron microscopy of metal halide perovskite materials. *ACS. Energy. Lett.* **2023**, *8*, 3048-53. DOI
119. Fan, Z.; Xiao, H.; Wang, Y.; et al. Layer-by-layer degradation of methylammonium lead tri-iodide perovskite microplates. *Joule* **2017**, *1*, 548-62. DOI
120. Akhavan, K. M. A.; Raval, P.; Cherednichekno, K.; et al. Molecular-level insight into correlation between surface defects and

stability of methylammonium lead halide perovskite under controlled humidity. *Small. Methods.* **2021**, *5*, e2000834. DOI

121. Draguta, S.; Sharia, O.; Yoon, S. J.; et al. Rationalizing the light-induced phase separation of mixed halide organic-inorganic perovskites. *Nat. Commun.* **2017**, *8*, 200. DOI PubMed PMC
122. Abdelmageed, G.; Jewell, L.; Hellier, K.; et al. Mechanisms for light induced degradation in $MAPbI_3$ perovskite thin films and solar cells. *Appl. Phys. Lett.* **2016**, *109*, 233905. DOI
123. Siegler, T. D.; Dunlap-Shohl, W. A.; Meng, Y.; et al. Water-accelerated photooxidation of $CH_3NH_3PbI_3$ perovskite. *J. Am. Chem. Soc.* **2022**, *144*, 5552-61. DOI
124. Song, Z.; Wang, C.; Phillips, A. B.; et al. Probing the origins of photodegradation in organic-inorganic metal halide perovskites with time-resolved mass spectrometry. *Sustain. Energy. Fuels.* **2018**, *2*, 2460-7. DOI
125. Liu, D.; Shao, Z.; Li, C.; Pang, S.; Yan, Y.; Cui, G. Structural properties and stability of inorganic $CsPbI_3$ perovskites. *Small. Struct.* **2021**, *2*, 2000089. DOI
126. Saliba, M.; Matsui, T.; Seo, J. Y.; et al. Cesium-containing triple cation perovskite solar cells: improved stability, reproducibility and high efficiency. *Energy. Environ. Sci.* **2016**, *9*, 1989-97. DOI PubMed PMC
127. Macpherson, S.; Doherty, T. A. S.; Winchester, A. J.; et al. Local nanoscale phase impurities are degradation sites in halide perovskites. *Nature* **2022**, *607*, 294-300. DOI
128. Deng, Y. H. Truth and myth of phase coexistence in methylammonium lead iodide perovskite thin film via transmission electron microscopy. *Adv. Mater.* **2021**, *33*, e2008122. DOI PubMed
129. Deng, Y. Common phase and structure misidentifications in high-resolution TEM characterization of perovskite materials. *Condens. Matter.* **2021**, *6*, 1. DOI
130. Kim, M.; Ham, S.; Cheng, D.; Wynn, T. A.; Jung, H. S.; Meng, Y. S. Advanced characterization techniques for overcoming challenges of perovskite solar cell materials. *Adv. Energy. Mater.* **2021**, *11*, 2001753. DOI
131. Ren, Z.; Mastropietro, F.; Davydok, A.; et al. Scanning force microscope for *in situ* nanofocused X-ray diffraction studies. *J. Synchrotron. Radiat.* **2014**, *21*, 1128-33. DOI
132. Bergmann, V. W.; Weber, S. A.; Javier, R. F.; et al. Real-space observation of unbalanced charge distribution inside a perovskite-sensitized solar cell. *Nat. Commun.* **2014**, *5*, 5001. DOI
133. Ferrer, O. J.; Tennyson, E. M.; Kusch, G.; et al. Using pulsed mode scanning electron microscopy for cathodoluminescence studies on hybrid perovskite films. *Nano. Ex.* **2021**, *2*, 024002. DOI
134. Hu, Q.; Zhao, L.; Wu, J.; et al. *In situ* dynamic observations of perovskite crystallisation and microstructure evolution intermediated from $[PbI_6]^{4-}$ cage nanoparticles. *Nat. Commun.* **2017**, *8*, 15688. DOI
135. Wang, H.; Liu, L.; Wang, J.; Li, C.; Hou, J.; Zheng, K. The development of iDPC-STEM and its application in electron beam sensitive materials. *Molecules* **2022**, *27*, 3829. DOI PubMed PMC
136. Bosch, E. G.; Lazic, I.; Lazar, S. Integrated differential phase contrast (iDPC) STEM: a new atomic resolution STEM technique to image all elements across the periodic table. *Microsc. Microanal.* **2016**, *22*, 306-7. DOI
137. Shen, B.; Wang, H.; Xiong, H.; et al. Atomic imaging of zeolite-confined single molecules by electron microscopy. *Nature* **2022**, *607*, 703-7. DOI
138. Xiong, H.; Liu, Z.; Chen, X.; et al. In situ imaging of the sorption-induced subcell topological flexibility of a rigid zeolite framework. *Science* **2022**, *376*, 491-6. DOI
139. Caswell, T. A.; Ercius, P.; Tate, M. W.; Ercan, A.; Gruner, S. M.; Muller, D. A. A high-speed area detector for novel imaging techniques in a scanning transmission electron microscope. *Ultramicroscopy* **2009**, *109*, 304-11. DOI
140. Tate, M. W.; Purohit, P.; Chamberlain, D.; et al. High dynamic range pixel array detector for scanning transmission electron microscopy. *Microsc. Microanal.* **2016**, *22*, 237-49. DOI
141. Han, Y.; Xie, S.; Nguyen, K.; et al. Picometer-precision strain mapping of two-dimensional heterostructures using an electron microscope pixel array detector (EMPAD). *Microsc. Microanal.* **2017**, *23*, 1712-3. DOI
142. Jiang, Y.; Chen, Z.; Han, Y.; et al. Electron ptychography of 2D materials to deep sub-ångström resolution. *Nature* **2018**, *559*, 343-9. DOI
143. Philipp, H.; Tate, M.; Shanks, K.; et al. Wide dynamic range, 10 kHz framing detector for 4D-STEM. *Microsc. Microanal.* **2021**, *27*, 992-3. DOI
144. Philipp, H. T.; Tate, M. W.; Shanks, K. S.; et al. Very-high dynamic range, 10,000 frames/second pixel array detector for electron microscopy. *Microsc. Microanal.* **2022**, *28*, 425-40. DOI
145. Scheid, A.; Wang, Y.; Jung, M.; et al. Electron ptychographic phase imaging of beam-sensitive all-inorganic halide perovskites using four-dimensional scanning transmission electron microscopy. *Microsc. Microanal.* **2023**, *29*, 869-78. DOI
146. Song, B.; Ding, Z.; Allen, C. S.; et al. Hollow electron ptychographic siffractive imaging. *Phys. Rev. Lett.* **2018**, *121*, 146101. DOI
147. Maiden, A. M.; Rodenburg, J. M. An improved ptychographical phase retrieval algorithm for diffractive imaging. *Ultramicroscopy* **2009**, *109*, 1256-62. DOI PubMed
148. Chen, Z.; Jiang, Y.; Shao, Y. T.; et al. Electron ptychography achieves atomic-resolution limits set by lattice vibrations. *Science* **2021**, *372*, 826-31. DOI
149. Aidukas, T.; Wechsler, F.; Loetgering, L.; Zhou, K.; Horstmeyer, R. Applications and extensions of fourier ptychography. *Microscopy. Today.* **2022**, *30*, 40-5. DOI